

MOLECULE FORMATION. II. IN INTERSTELLAR SHOCK WAVES

P. A. AANNESTAD

Institute for Space Studies, Goddard Space Flight Center, NASA, New York

Received 1972 May 3

ABSTRACT

We study the processes of grain destruction and molecule formation due to the sputtering of grain mantles as the grains move relative to the gas in the hot shock wave. It is found that mantles are destroyed completely by this process if the abundance of molecular hydrogen is about 1 percent or more; the corresponding lifetime of a mantle is about 5×10^7 years. We follow the variation of the molecular species through the shock wave using the sputtering process as a source for H_2O , NH_3 , and CH_4 . It is found that OH and H_2O may attain an abundance $\sim 10^{-5}$ relative to H, but only over a narrow region about 10^{-3} pc immediately behind the shock front. For clouds of 200–500 M_\odot the column densities are about 10^{13} cm^{-2} for OH and 10^{12} cm^{-2} for H_2O . The molecules CO, CN, and CH are found to be very abundant (10^{-4} to 10^{-6} relative to H) in the cold ($\sim 10^\circ$ K) and dense ($\sim 10^4$ to 10^5 cm^{-3}) region far behind the shock front. Column densities are 10^{13} to 10^{14} cm^{-2} through the shock wave, but will increase by at least an order of magnitude as the wave travels through a cloud.

We study the cooling processes in the shock, including the effect of OH and H_2O . It is found that cooling by molecules other than H_2 is not important, except for CO, which may be the main cooling agent in the cold and dense region. We treat cooling by both ortho- and para- H_2 , and it is found that the $6.9\text{-}\mu$ ($J = 7 \rightarrow 5$) transition of ortho- H_2 gives the strongest H_2 line for a wide range of shock velocities. For shock velocities greater than about 15 km s^{-1} , we find that collisional dissociation of H_2 decreases the strength of the rotational lines substantially.

Subject headings: abundances, nebular — interstellar matter — molecules, interstellar — shock waves

I. INTRODUCTION

In a previous paper (Aannestad 1973; hereafter referred to as Paper I) we studied molecule formation during the quiescent evolution of interstellar clouds. We showed that interstellar grains will grow methane-ice mantles out of the cooling elements of the gas, causing a cloud to heat up and expand, and we followed the variations in temperature, density, and atomic and molecular abundances. There is some observational evidence (Howard, Wentzel, and McGee 1963) that the depletion of heavy elements is small in certain cases, indicating that mantle material is now and then restored to the gas phase. Energetic events like cloud-cloud collisions and clouds encountering H II regions may cause such removal of grain material. Oort and van de Hulst (1946) studied grain-grain collisions as a means of obtaining an equilibrium size distribution for the interstellar grains. However, interpenetration of grains in different clouds may be hindered drastically by the very high densities in the cold and dense regions behind the shock front which inevitably accompany cloud collisions (Spitzer 1968; and see § VIII herein). Another destruction process for the grains is sputtering by hot atoms as the grains are overrun by the shock wave. This has been treated by Wickramasinghe (1965) and by Gidalevich (1966*a, b, c*, 1967) with very simplified assumptions as to the structure of the shock wave and the interaction between hot gas atoms and the interstellar grains. In particular, these authors neglected the influence of the relative motion between grains and gas on the destruction of the grains. Zimmermann (1970) has studied in detail the dynamical separation between

gas and dust, but neglected the sputtering process. In this work we treat both of these processes in detail together with a realistic shock structure.

Shock waves may also be a way of forming interstellar molecules. Stecher and Williams (1966) proposed that chemical exchange reactions could form CH, CH⁺, OH, and CN, but found disagreement with observations by more than two orders of magnitude. They found, however, that agreement could be obtained near early-type stars where the grains are driven at supersonic speeds through the gas by the radiation pressure. Field, Aannestad, and Solomon (1968) studied gas-phase reactions in shock waves for the formation of OH, but found disagreement with observation by about two orders of magnitude unless H₂ was very abundant (H₂/H > 10⁻³). It was suggested by Dieter and Goss (1966) that maybe OH is derived from H₂O as the latter is sputtered off the grains in hot shock fronts. In the present work we investigate in detail both hot gas-phase reactions and the destruction of grains as a source for simple molecules in interstellar space.

We treat shock waves in clouds whose precollision history has been calculated in Paper I. In § II we discuss the shock structure, and in § III the dynamics of the grains is considered. In § IV we treat in some detail the process of sputtering, and in § V we give expressions for the cooling rates, including cooling due to the molecules formed behind the shock front. In § VI we give all the chemical reactions included in the calculations. The results of calculations for a range of shock velocities and initial molecular hydrogen abundances are given in § VII, while the discussion is in § VIII.

II. SHOCK STRUCTURE

The treatment of the shock structure is considerably simplified by idealizing to the case of a uniform gas being shocked by an infinite piston which has proceeded into the gas for a time much longer than the relaxation times we discuss below. This permits the assumption of a steady state for the variables far downstream from the shock. This assumption has been verified by initial-value calculations by Mészáros (private communication). We study a steady shock in the compression phase only in much the same way as done by Field *et al.* (1968; hereafter referred to as FRAO) and neglect the effects of the expansion phase as found by Stone (1970*a, b*). We will furthermore neglect the magnetic field, which is equivalent to the piston moving parallel to the magnetic field. As shown by the results of FRAO, a perpendicular field comparable to the observed value of ~3 microgauss affects the shock structure and the timescales involved by less than 50 percent. Its effect on the grain motion may, however, be important (see § VIII).

Since our shock speeds are $\lesssim 20 \text{ km s}^{-1}$, corresponding to 0.16 rydbergs, we neglect ionization of hydrogen by thermal collisions, and therefore there is no radiative precursor. The shock structure (Whitney and Skalafuris 1963; Hurlle 1967) is then composed of the following regions: (i) the region where translational degrees of freedom are excited (defined to be the shock front); (ii) the region where internal degrees of freedom are excited, such as fine structure, rotation, and vibration; and (iii) the region where chemical reactions and radiative losses occur.

Following FRAO, we note that region (i) is much thinner than any of the other regions (corresponding to a few mean free paths $\sim 10^{-5}$ pc) and may be treated as a discontinuity. Region (ii) is thicker than region (i), with the vibrational mode being the least coupled to the translational degrees of freedom. Nevertheless, we have treated region (ii) as a discontinuity and assumed instantaneous response of level populations to changes in temperature, density, and molecular abundances. Region (iii) encompasses reactions with widely different cross-sections and is thus not a uniformly relaxing region. However, the chemical reactions have generally larger cross-sections than the inelastic cross-sections that define region (ii), although in a

few cases they may be comparable. FRAO showed that the size of region (iii) as defined by the cooling rate justified a detailed treatment of region (iii) while treating region (ii) as a discontinuity. This may not be so in our case, since the fastest reactions involved have rates $\sim 10^{-9} n_{\text{H}}$, of the same order as the excitation rates in region (ii). However, except for H_2 , we will show that the influence of the molecules on the cooling rate is small, so that this difference in treatment is not likely to change the structure of the shock. For H_2 the collisional dissociation rate is $\sim 10^{-10} \text{ s}^{-1}$ immediately behind the shock front, while the excitation rate is 10^{-9} to 10^{-10} s^{-1} , so that the assumption of equilibrium in region (ii) may not be accurate in this case.

Assuming an ideal gas, one may show (FRAO, eq. [10]) that the time since a given element of gas passed through the shock front is given by

$$t(y) = -\frac{R\rho_1}{\mu} \int_{y_2}^y \frac{y^2}{T(y)^{1/2}\Lambda(y,T(y))} d\left[\frac{T(y)^{3/2}}{y}\right], \quad (1)$$

where we have introduced the density ratio $y = \rho/\rho_1$ as the independent variable and the subscripts 1 and 2 denote the preshock region and the region immediately behind the shock front, respectively, R is the gas constant, and μ is the molecular weight. Ignoring radiative self-absorption, the loss rate Λ is a point function of density and temperature given by

$$\Lambda = \Lambda(y, T) = \sum_i \Lambda_i + \sum_r \Lambda_r, \quad (2)$$

where Λ_i denotes the loss rate due to a given emission line and Λ_r denotes the loss rate due to a given chemical reaction. In general, we may ignore the influence of the chemical reactions on the energy balance, except for H_2 , where collisional dissociation occurs fast in the hot shock region (if $T \gtrsim 8000^\circ \text{ K}$), removing 4.5 eV for every dissociation. The various terms contributing to Λ are given in § V.

From conservation of mass and momentum, the temperature at any point behind the shock wave is given by

$$T(y) = \frac{T_1}{y} + \frac{\mu v_1^2}{R} \frac{y-1}{y^2}, \quad (3)$$

where v_1 is the speed of the preshock gas with respect to the shock front. From energy conservation through the shock front, the density ratio y_2 is given by

$$y_2 = \frac{(\gamma+1)v_1^2}{(\gamma-1)v_1^2 + 2\gamma c^2}, \quad (4)$$

where c is the isothermal sound speed in the preshock region and γ is the ratio of specific heats, $\gamma = \frac{5}{3}$. Since the shock structure as a whole is nearly an isothermal shock, $v_1 \approx \frac{1}{2}V$, where V is the total relative speed in a given cloud-cloud collision. Thus, by specifying $V = 2v_1$, ρ_1 , and T_1 , equation (1) may be integrated and this gives together with equation (3) the cooling curve $T(t)$. Also knowing $y(t)$, the intensity (ergs $\text{cm}^{-2} \text{ sec}^{-1} \text{ sterad}^{-1}$) of an emission line may be calculated via

$$I_i = \frac{v_1}{4\pi} \int_0^\tau \frac{\Lambda_i[y(t), T(t)]}{y(t)} dt. \quad (5)$$

Here τ denotes the ‘‘cooling time,’’ which is the time at which the cloud is again in thermal equilibrium, with the radiative losses being balanced by the heating processes. We shall find, however, that in general this timescale is somewhat longer than the time

at which depletion would again become important in the cool and dense region. Since we neglect resumed depletion in the postshock phase, we therefore terminate the calculations before actual thermal equilibrium has been achieved. In all cases, however, the clouds cool down to temperatures significantly lower than the preshock temperature.

III. DYNAMICS OF GRAINS

As a grain has a much larger inertia than a gas atom, it will experience a velocity relative to the gas as it goes through the shock front of $U = v_1 - v_2$. In the cooling region, a charged grain will in general be acted upon by three forces: (i) a magnetic force due to a magnetic-field component normal to the shock velocity; (ii) a Coulomb drag force due to the interaction of the grain with the free ions in the gas; and (iii) a gas-kinetic drag force due to the compressed, hot, and neutral gas. Since we have assumed a parallel magnetic field, there is no contribution from (i), but we will show (§ VIII) that a perpendicular field may effectively couple grains and gas behind the shock front.

Using the expression derived by Spitzer (1962) for the plasma drag, we find that only if the fractional ionization is about 10 percent or more would the plasma drag dominate the kinetic drag in the hot shock region. Since the cooling time is much smaller than the relaxation time for cosmic-ray ionization, the actual ionization is "frozen" to the preshock value of ~ 0.2 percent, and we have therefore neglected the plasma drag in the motion of the grain.

The kinetic drag due to neutral atoms of density n and mass m has been shown by Baines, Williams, and Asebiomo (1965) to be

$$F_k = \pi^{1/2} a^2 n m V_n^2 G_n, \quad (6)$$

where a is the grain radius, $V_n = (2kT/m)^{1/2}$, and G_n is a function only of the speed ratio U/V_n , defined as

$$G_n(x) \equiv \left(x + \frac{1}{2x}\right) \exp(-x^2) + \pi^{1/2} \left(x^2 + 1 - \frac{1}{4x^2}\right) \operatorname{erf}(x) + \frac{1}{3}\pi x.$$

Since G_n is approximately $\propto U/V_n$ for $U/V_n \approx 1$, we see that $F_k \propto nm^{1/2}$ and helium atoms would thus contribute a force about 18 percent of that of the H atoms. In the calculations, we have included this contribution, so that the total force is $F = F_{k,H} + F_{k,He}$, where F_k is given by equation (6). If u is the speed of the grain relative to the shock front at a time t_{gr} since it passed through the shock front, then as $F = -m_{gr} du/dt_{gr}$ and $du/dt_{gr} = (u/v)(du/dy)/(dt/dy)$, the grain motion is governed by

$$\frac{du}{dy} = -m_{gr}^{-1} \left(\frac{v}{u}\right) \left(\frac{dt}{dy}\right) F, \quad (7)$$

where v is the gas speed relative to the shock front and dt/dy is given by equation (1).

IV. SPUTTERING

Mathews (1969) employed a yield function for sputtering indicated by experimental data for normal incidence. Unfortunately, he inadvertently employed a value for the proportionality constant that was a factor of 10^3 too large.¹ Such corrections would make the sputtering process negligible even in dense H II regions. However, normal incidence sputtering requires at least two collisions for sputtering to occur, while a

¹ This has been independently pointed out by Barlow (1971).

single collision may be sufficient for oblique incidence. Low-energy normal incidence sputtering is therefore inherently different and less efficient than oblique incidence sputtering, and the experimental value of the proportionality constant for normal incidence may not be representative for any other angle. Experiments on the influence of the angle of incidence on sputtering yields (Wehner 1959; Molchanov and Telkovskii 1961) show that the angle effect, although depending upon the metals involved, may be quite pronounced. For molybdenum the maximum yield at 40° incidence was 16 times higher than the yield at normal incidence. Although these experiments have been done only for high incident energies (200–800 eV), any angle effect would probably be enhanced for energies closer to the threshold energy.

Using the expression deduced by Henschke (1957) for the threshold energy at oblique incidence, but assuming a spherically symmetric potential barrier, we have adopted the following expression for the threshold energy as a function of the angle of incidence ($I \equiv 0$ at grazing incidence):

$$E_{\text{th}}(I) = \frac{(m + M)^2}{(1 + \delta)^2 m M} \frac{\varphi}{\sin^2(\gamma_m - I)}. \quad (8)$$

Here M is the mass of the target particle, m is the mass of the incident particle, φ is the binding energy of the target material, and δ is an energy dissipation factor ($\delta \equiv 1$ for a completely elastic sputtering process). Although for a given I the ejection angle γ may have a range of values (Appendix), we have here assumed that the effective threshold energy is described by the maximum value of γ given by $\cos \gamma_m = 2r_M/c$, where r_M is the hard-sphere collision radius of surface particles separated by a distance c . The maximum value of I is $I_m = \gamma_m (\approx 75^\circ)$, so that $E_{\text{th}} \rightarrow \infty$ as $I \rightarrow I_m$, reflecting the fact that the incident direction is then normal to the ejection direction so that no net momentum can be transferred. At such large angles, however, normal incidence sputtering will probably occur, causing the actual threshold energy to level off with increasing I , in the manner more or less described by the relation used by Mathews. The angle-dependent term in equation (8) gives a smaller threshold energy (by a factor of 2) than the corresponding term in Mathews's relation as long as $I \lesssim 60^\circ$. Since we will find that the yield function peaks strongly at lower angles of incidence, we have restricted ourselves to the use of equation (8) only.

Assuming a linear dependence on energy, we then write for the yield function

$$Y(E, I) = k P_g(I) \frac{E - E_{\text{th}}(I)}{E_{\text{th}}(I)}, \quad (9)$$

where $P_g(I)$ is a function determined from geometric considerations in the Appendix and k is a nondimensional proportionality constant to be estimated from experiments. Employing equation (8), we find

$$Y(E, I) = \frac{(1 + \delta)^2 m M k}{(M + m)^2 \varphi} P(I) [E - E_{\text{th}}(I)], \quad (10)$$

where $P(I) \equiv P_g(I) \sin^2(\gamma_m - I)$.

We have compared equation (10) with experimental data for Hg^+ impinging on Mo (Wehner 1959). The yield has a sharp peak at about the same angle as in the data ($\approx 40^\circ$) if $c = 2^{1/4}d$, where d is the nearest-neighbor distance, and gives a correct maximum yield if $k \approx 10$. However, the yield function is quite a bit narrower than suggested by the data. This effect may be expected, since we have employed only a single distance between the surface particles, while, in reality, there will be a distribution of such distances, depending on surface orientation and the state of damage of the

TABLE 1
THE "YIELD" Y' FOR He SPUTTERING OF H₂O

RELATIVE VELOCITY [km s ⁻¹]	TEMPERATURE [° K]									
	1000	2000	3000	4000	5000	6000	7000	8000	9000	10,000
18.....	22	16	14	13	12	11	11	10	10	10
17.....	18	13	11	10	9.7	9.3	9.0	8.8	8.7	8.6
16.....	14	10	9.1	8.3	7.9	7.6	7.5	7.3	7.3	7.2
15.....	11	8.1	7.1	6.6	6.4	6.2	6.1	6.0	6.0	6.0
14.....	7.8	6.1	5.5	5.2	5.0	4.9	4.9	4.9	4.9	5.0
13.....	5.5	4.4	4.1	3.9	3.9	3.9	3.9	3.9	4.0	4.0
12.....	3.6	3.0	2.9	2.9	2.9	3.0	3.0	3.1	3.2	3.3
11.....	2.1	2.0	2.0	2.0	2.1	2.2	2.3	2.4	2.5	2.6
10.....	1.1	1.2	1.3	1.4	1.5	1.6	1.7	1.8	1.9	2.0
9.....	0.49	0.65	0.79	0.92	1.0	1.1	1.3	1.4	1.5	1.6
8.....	0.17	0.32	0.45	0.57	0.69	0.80	0.91	1.0	1.1	1.2
7.....	0.044	0.14	0.24	0.34	0.44	0.54	0.63	0.73	0.83	0.93
6.....	0.0085	0.052	0.12	0.19	0.30	0.35	0.44	0.52	0.61	0.70
5.....	0.0012	0.017	0.052	0.10	0.16	0.23	0.30	0.37	0.45	0.53
4.....	0.00011	0.0049	0.022	0.052	0.093	0.14	0.20	0.26	0.33	0.40
3.....	0.000008	0.0012	0.0086	0.026	0.054	0.091	0.14	0.19	0.25	0.31
2.....	0.0000004	0.00028	0.0034	0.013	0.032	0.060	0.097	0.14	0.19	0.25
1.....	0.00000002	0.00007	0.0015	0.0076	0.022	0.044	0.076	0.12	0.16	0.22

surface. Clearly, we have no way of knowing what the distribution of nearest-neighbor distances is for an interstellar grain, so that this effect must be accommodated in the proportionality factor k . Requiring that the integral under the predicted yield curve equals the integral under the observed curve for Mo gives a value of $k \approx 50$.

The total number of sputtered particles per unit time from a grain of radius a moving with velocity U in a gas of density n , temperature T , and composed of particles p with mass m and charge Z is found to be

$$S_p = \left(\frac{8\pi kT}{m}\right)^{1/2} a^2 n e^{-mU^2/2kT} \int_{I_0}^{I_m} \sin I \cos I dI \int_{\epsilon_m}^{\infty} (\epsilon + Z\Gamma) Y(I, \epsilon + Z\Gamma) e^{-\epsilon} d\epsilon \\ \times \int_0^\pi B_0(2X\epsilon^{1/2} \cos I \sin \theta) \exp(2X\epsilon^{1/2} \sin I \cos \theta) \sin \theta d\theta. \quad (11)$$

Here B_0 is the modified Bessel function $B_0(z) \equiv J_0(iz)$, and the yield Y is given by equation (10) with $E = (\epsilon + Z\Gamma)kT$, where Γ is the parameter characterizing the charge on the grain ($Z_{\text{gr}}e$), $\Gamma \equiv -Z_{\text{gr}}e^2/(akT)$. I_0 is given by equation (A3), and I_m is given by $\cos I_m = 2r_M/c$. X is the speed ratio $U/(2kT/m)^{1/2}$, and $\epsilon_m \equiv \max(0, E_{\text{th}}/kT - Z\Gamma)$.

The most important sputtering agents are H, H⁺, and He, He⁺, He⁺⁺, and Ne. To compare the various contributions, we evaluated equation (11) numerically for $T = 4200^\circ \text{K}$, $U = 5 \text{ km s}^{-1}$, which are typical values in the hot region behind the shock front. We assumed that $\delta = 0.5$ and that the collision radii are 1 Å for H₂O, CH₄, He, and Ne, 0.5 Å for H and He⁺, and zero for H⁺ and He⁺⁺. Expecting interstellar mantles to be quite amorphous, we assumed that the distance $c = 7.55 \text{ Å}$. However, such a distance leads to a density lower than 1.5 g cm^{-3} , which we employed in the treatment of grain growth (Paper I), and future calculations should take this into account. The binding energies of H₂O and CH₄ have been taken to be 0.28 and 0.06 eV, respectively. Taking account of the relative abundances and assuming cosmic-ray ionization, we find that the sputtering rate of H₂O relative to that by H is 0.15,

TABLE 2
THE "YIELD" Y' FOR He SPUTTERING OF CH₄

RELATIVE VELOCITY [km s ⁻¹]	TEMPERATURE [° K]									
	1000	2000	3000	4000	5000	6000	7000	8000	9000	10,000
18.....	225	164	138	124	115	109	104	100	98	95
17.....	189	138	118	106	98	93	90	87	85	83
16.....	157	116	99	90	84	80	77	75	73	72
15.....	129	96	83	75	70	67	65	64	62	62
14.....	105	79	68	62	59	57	55	54	53	53
13.....	84	63	55	51	49	47	46	45	45	45
12.....	66	50	45	41	40	39	38	38	38	38
11.....	50	39	35	33	32	32	31	31	32	33
10.....	38	30	27	26	26	26	26	26	26	27
9.....	27	22	21	20	20	20	21	21	22	22
8.....	19	16	16	16	16	16	17	17	18	18
7.....	13	11	11	12	12	13	13	14	15	15
6.....	8	8	8	9	9	10	11	11	12	13
5.....	4	5	6	6	7	8	8	9	10	10
4.....	2	3	4	4	5	6	7	7	8	9
3.....	1	2	3	3	4	5	5	6	7	8
2.....	0.3	1	2	2	3	4	5	5	6	7
1.....	0.1	0.6	1	2	3	3	4	5	6	6

TABLE 3
THE "YIELD" Y' FOR H SPUTTERING OF CH_4

RELATIVE VELOCITY [km s^{-1}]	TEMPERATURE [$^{\circ}$ K]									
	1000	2000	3000	4000	5000	6000	7000	8000	9000	10,000
18.....	11	9	9	9	9	9	9	9	10	10
17.....	9	8	7	7	8	8	8	8	9	9
16.....	7	6	6	6	7	7	7	8	8	8
15.....	6	5	5	5	6	6	6	7	7	7
14.....	4	4	4	5	5	5	6	6	6	7
13.....	3	3	4	4	4	5	5	5	6	6
12.....	2	3	3	3	4	4	4	5	5	5
11.....	2	2	2	3	3	3	4	4	5	5
10.....	1	1	2	2	3	3	3	4	4	4
9.....	0.6	1	1	2	2	3	3	3	4	4
8.....	0.4	0.8	1	2	2	2	3	3	3	4
7.....	0.2	0.5	0.9	1	2	2	2	3	3	3
6.....	0.1	0.4	0.7	1	1	2	2	2	3	3
5.....	0.06	0.3	0.5	0.8	1	2	2	2	3	3
4.....	0.03	0.2	0.4	0.7	1	1	2	2	2	3
3.....	0.01	0.1	0.3	0.6	0.9	1	2	2	2	3
2.....	0.006	0.09	0.3	0.5	0.8	1	1	2	2	2
1.....	0.003	0.07	0.3	0.5	0.8	1	1	2	2	2

61, 3, 0.05, and 4 for H^+ , He, He^+ , He^{++} , and Ne, respectively. Thus, He dominates the sputtering of H_2O by an order of magnitude, and we thus neglect sputtering of H_2O by any particles other than He. In the case of sputtering of CH_4 , we find that H dominates the sputtering rates, being about a factor of 3 more effective than He. For lower temperatures He will again dominate over H, but we include sputtering by both H and He of CH_4 throughout the calculation.

Using the parameters given above, we have numerically evaluated the "yield" $Y'(T, U)$ defined via $Y' \equiv S_p(T, U)/(n\bar{v}\pi a^2)$, where \bar{v} is the mean speed in the gas. In tables 1–3 we show Y' for a grid of (T, U) values. In the case of the sputtering of CH_4 , we see that the "yield" becomes very large for high values of T and U , due to our assumption that the yield is a linear function of energy, which is shown by experiments to break down when the yield is ~ 10 –15. Thus, the largest yield values in table 2 are probably overestimated. However, since most of our cases will not employ the extreme (T, U) values, the practical effects of this may not be serious.

V. COOLING MECHANISMS

The first cooling mechanism to be considered is that of the fine-structure transitions. Expressions for the cooling rates due to excitation of fine-structure levels in O^0 , C^+ , Fe^+ , and Si^+ by collisions with hydrogen atoms and electrons were calculated by FRAO, who assumed the spin exchange probability to be $\frac{2}{3}$. Bahcall and Wolf (1968) have given more general expressions for this probability, also accounting for the cases where the fine-structure splitting is not small compared with kT . Using the latter expressions and neglecting collisional deexcitation, we find the following cooling rates ($\text{erg cm}^{-3} \text{ s}^{-1}$):

$$\Lambda(\text{C}^+, 156\mu) = (7.89 \times 10^{-20} T^{-1/2} n_e + 1.66 \times 10^{-23} n_{\text{H}}) e^{-92/T} n(\text{C}^+), \quad (12)$$

$$\Lambda(\text{Si}^+, 35\mu) = (1.89 \times 10^{-18} T^{-1/2} n_e + 7.45 \times 10^{-23} n_{\text{H}}) e^{-413/T} n(\text{Si}^+), \quad (13)$$

$$\Lambda(\text{Fe}^+, 35\mu) = (5.9 \times 10^{-19} T^{-1/2} n_e + 1.9 \times 10^{-23} n_{\text{H}}) e^{-961/T} n(\text{Fe}^+), \quad (14)$$

$$\Lambda(\text{Fe}^+, 26\mu) = \{[1.1 \times 10^{-18}T^{-1/2}n_e + 1.2 \times 10^{-22}(0.56 - 0.14e^{-407/T})n_{\text{H}}]e^{-554/T} + [8 \times 10^{-19}T^{-1/2}n_e + 2.6 \times 10^{-23}n_{\text{H}}]e^{-961/T}\}n(\text{Fe}^+), \quad (15)$$

$$\Lambda(\text{O}^0, 147\mu) = 5.3 \times 10^{-25}T^{-1/6}e^{-326/T}n_{\text{H}}n(\text{O}^0), \quad (16)$$

and

$$\Lambda(\text{O}^0, 63\mu) = [1.24 \times 10^{-24}e^{-326/T} + 6.7 \times 10^{-24}e^{-228/T}(0.625 - 0.069e^{-98/T})] \times T^{1/6}n_{\text{H}}n(\text{O}^0). \quad (17)$$

The cooling rates for C^+ and O^0 correspond well with recent calculations by Wofsy, Reid, and Dalgarno (1971).

Neutral carbon cooling may be important in the low-temperature, high-density region far behind the shock front where recombination of C^+ with electrons occurs efficiently. This region was not studied by FRAO. From the expressions given by Bahcall and Wolf (1968), using the Einstein A values as given by Wiese, Smith, and Glennon (1966), we find for the cooling rates due to fine-structure excitation of neutral carbon

$$\Lambda(\text{C}^0, 369\mu) = 1.37 \times 10^{-24}T^{1/6}e^{-63/T}n_{\text{H}}n(\text{C}^0) \quad (18)$$

and

$$\Lambda(\text{C}^0, 610\mu) = [8.3 \times 10^{-25}e^{-63/T} + 4.48 \times 10^{-24}e^{-24/T}(0.25 - 0.14e^{-39/T})] \times T^{1/6}n_{\text{H}}n(\text{C}^0). \quad (19)$$

The importance of collisional deexcitation is measured by the ratio C/A , where C is the collisional deexcitation rate and A is the Einstein A value. For C^+ , $C/A \approx 10^{-4}n_{\text{H}}$, and we have corrected for collisional deexcitation when $n_{\text{H}} \geq 300 \text{ cm}^{-3}$. For the species Si^+ , O^0 , and C^0 we have taken deexcitation into account whenever $n_{\text{H}} \geq 10^3 \text{ cm}^{-3}$, while no correction was applied to the transitions of Fe^+ since these have such large A values, $\geq 10^{-3} \text{ s}^{-1}$, that collisional deexcitation is not important for the range of densities treated here ($n_{\text{H}} \lesssim 10^5 \text{ cm}^{-3}$).

In addition to the fine-structure transitions, we have included the additional cooling terms as suggested by Habing and Goldsmith (1971):

$$\Lambda(\text{Fe}^+, 5.4 \mu) = 4.8 \times 10^{-18}T^{-1/2}e^{-2740/T}n_e n(\text{Fe}^+), \quad (20)$$

$$\Lambda(\text{Fe}^+, 4.1 \mu) = 6.6 \times 10^{-18}T^{-1/2}e^{-3540/T}n_e n(\text{Fe}^+), \quad (21)$$

$$\Lambda(\text{O}^0, 6300 \text{ \AA}) = 1.9 \times 10^{-22}T^{1/3}e^{-22,700/T}n_e n(\text{O}^0), \quad (22)$$

and

$$\Lambda(\text{N}^0, 5201 \text{ \AA}) = 1.1 \times 10^{-21}T^{1/2}e^{-27,700/T}n_e n(\text{N}^0). \quad (23)$$

We next consider cooling due to the collisional excitation of H_2 molecular rotation by H atoms. Nishimura (1968) has calculated transition rate coefficients for both para- and ortho- H_2 for all transitions up to $J = 15$. The inherent uncertainty in the calculations due to the uncertainty in the potential surface (Tang 1969) will only affect the highest levels, since the lower levels are nearly in thermal equilibrium at the densities considered. In computing the loss rates, we have followed the procedure as outlined by FRAO. The energy levels, the wavelengths of the transitions, and the

Einstein A values are listed in table 4. The A values for para- H_2 deviate slightly from the values given by FRAO. This is because the latter were calculated from a one-term approximation to the energy separation of the levels, while we have here used the more exact energies as determined from experimental data summarized by Field, Sommerville, and Dressler (1966).

As pointed out by FRAO, cooling by molecules may be important in the hot region immediately behind the shock front. We limit ourselves to the two species OH and H_2O since in our calculations we expect these to be among the most abundant molecules in the hot region, and we first discuss rotational excitation of OH by H atoms. Since the shock wave heats the gas to temperatures of several thousand degrees, the rotational spacings in OH are much smaller than kT , and we would expect a situation similar to that of NO and I_2 at room temperature where large multiple quantum jumps have been observed (Broida and Carrington 1963; Steinfeld and Klemperer 1965). For our purpose it suffices to make use of the suggestion (Callear and Lambert 1969) that the probabilities of multiple transitions are limited by the transitional overlap integral. We assume that the probability of a transition $J' \rightarrow J = J' + \Delta J$ is governed by

$$P(J' \rightarrow J' + \Delta J) \propto \frac{2(J' + \Delta J) + 1}{2J' + 1} \exp [-(3/2)A - \Delta E/2kT], \quad (24)$$

where $A = (4\pi^2\mu l^2 \Delta E^2 / \hbar^2 kT)^{1/3}$, μ is the reduced mass of the collision partners, and l is the characteristic distance in the interaction potential, $l = 0.2 \text{ \AA}$ (Herzfeld and Litovitz 1959, p. 328). If we compare equation (24) with the ratios $P(\Delta J)/P(\Delta J = 2)$ for the experimental transition probabilities of He^3 exciting I_2 as determined by Steinfeld and Klemperer (1965), we find that it reproduces the data to within 30 percent as long as $\Delta J \leq 10$. For larger values of ΔJ it overestimates the transition probabilities, and the relative probability is too large by a factor of 3 for $\Delta J = 20$.

Following Takayanagi and Nishimura (1960), we have assumed that the transition probability between the two lowest levels in the $^2\pi_{3/2}$ ladder is 0.5 for kinetic energies

TABLE 4
ROTATIONAL TRANSITIONS IN THE H_2 MOLECULE

Transition ($J =$)	Excitation $E(J)/k$ [° K]	Wavelength $\lambda(J \rightarrow J - 2)$ [μ]	$A(J \rightarrow J - 2)^*$ [s^{-1}]
2 \rightarrow 0.....	510	28.2174	2.9×10^{-11}
3 \rightarrow 1.....	1015	17.0345	4.6×10^{-10}
4 \rightarrow 2.....	1682	12.2788	2.6×10^{-9}
5 \rightarrow 3.....	2504	9.6651	9.3×10^{-9}
6 \rightarrow 4.....	3475	8.0246	2.4×10^{-8}
7 \rightarrow 5.....	4587	6.9074	5.3×10^{-8}
8 \rightarrow 6.....	5832	6.1033	1.0×10^{-7}
9 \rightarrow 7.....	7203	5.5005	1.7×10^{-7}
10 \rightarrow 8.....	8690	5.0337	2.7×10^{-7}
11 \rightarrow 9.....	10,289	4.6617	4.0×10^{-7}
12 \rightarrow 10.....	11,993	4.3571	5.6×10^{-7}
13 \rightarrow 11.....	13,798	4.1004	7.7×10^{-7}
14 \rightarrow 12.....	15,704	3.8767	1.0×10^{-6}
15 \rightarrow 13.....	17,713	3.6746	1.4×10^{-6}

* In computing the A values we have employed a value of the quadrupole moment of H_2 of $0.48067 ea_0^2$, determined from the work by Kolos and Roothan (1960; note that the first term in their eq. [29] is to be multiplied by a factor of $\frac{1}{2}$ [Field, personal communication]).

above threshold. The energy levels were taken from the work by Dieke and Crosswhite (1962). To calculate the collisional excitation rate between OH and H we have assumed elastic cross-sections as given by a van der Waals interaction, so that

$$\langle vQ(J' \rightarrow J' + \Delta J) \rangle = 1.5 \times 10^{-10} c^{1/3} T^{1/6} P(J' \rightarrow J' + \Delta J). \quad (25)$$

Here c is now the van der Waals constant corrected for the dipole-induced dipole contribution, $c(\text{OH}, \text{H}) \approx 15$ a.u. The total loss rate due to collisional excitation of OH by H atoms as employed in the calculations is

$$\begin{aligned} \Lambda_{\text{rot}}(\text{OH}, \text{H}) = & n_{\text{OH}} n_{\text{H}} \sum_{J=5/2}^{23/2} \langle vQ(3/2 \rightarrow J) \rangle \Delta E(3/2, J) \\ & + n_{\text{OH}} n_{\text{H}} \sum_{J=1/2}^{19/2} \langle vQ(3/2 \rightarrow J) \rangle \Delta E(3/2, J), \end{aligned} \quad (26)$$

where the first sum refers to the transitions from the ground state ($J' = 3/2$) within the ${}^2\pi_{3/2}$ ladder, and the second sum refers to the transitions out of the ground state and into the ${}^2\pi_{1/2}$ ladder.

In the case of rotational excitation of H_2O by H we have again used equations (24) and (25), assuming that H_2O is formed in the hot gas according to the ratio of the statistical weights of the energy levels. We have included all levels with energies less than 2000 cm^{-1} . The energy levels were taken from the work by Benedict, Claassen, and Shaw (1952). As in the case of OH, we assumed that the probability of the transition $0_0 \rightarrow 1_0$ is 0.5 and scaled all other probabilities according to equation (24). The corrected van der Waals constant is $c(\text{H}, \text{H}_2\text{O}) = 23$ a.u. The total cooling rate due to collisional excitation of H_2O by H is then

$$\begin{aligned} \Lambda_{\text{rot}}(\text{H}_2\text{O}, \text{H}) = & 0.75 n_{\text{H}_2\text{O}} n_{\text{H}} \sum_{J_i=2-1}^{12-7} \langle vQ(1_{-1} \rightarrow J_i) \rangle \Delta E(1_{-1}, J_i) \\ & + 0.25 n_{\text{H}_2\text{O}} n_{\text{H}} \sum_{J_i=1_0}^{12-10} \langle vQ(0_0 \rightarrow J_i) \rangle \Delta E(0_0, J_i), \end{aligned} \quad (27)$$

where the first sum refers to the excitation of the antisymmetric species and the second sum to the symmetric species of H_2O .

We now consider rotational excitation of OH and H_2O by electrons. Goss and Field (1968) have given rate constants for downward collisions between polar molecules and electrons in terms of a tabulated function $F(z)$, where z is proportional to the mean electron velocity. We may neglect quantum corrections and all strong collisions so that the cooling rate ($\text{ergs cm}^{-3} \text{ s}^{-1}$) due to rotational excitation of OH by electrons is given by

$$\Lambda_{\text{rot}}(\text{OH}, e) = [6.0 \times 10^{-21} F(z_1) e^{-120/T} + 3.3 \times 10^{-21} F(z_2) e^{-182/T}] n(\text{OH}) n_e. \quad (28)$$

Here z_1 refers to the ${}^2\pi_{3/2}(J = 3/2 \rightarrow 5/2)$ transition and is given by $z_1 = 0.18T^{1/2}$, and z_2 refers to the ${}^2\pi_{3/2}(J = 3/2) \rightarrow {}^2\pi_{1/2}(J = 1/2)$ transition and is given by $z_2 = 0.14T^{1/2}$. For the loss rate due to rotational excitation of H_2O by electrons, taking account of the two different symmetry species, we have

$$\Lambda_{\text{rot}}(\text{H}_2\text{O}, e) = [5 \times 10^{-21} F(z_1) e^{-54/T} + 2.1 \times 10^{-20} F(z_2) e^{-114/T}] n(\text{H}_2\text{O}) n_e. \quad (29)$$

Here z_1 refers to the $0_0 \rightarrow 1_0$ transition and is given by $z_1 = 0.20T^{1/2}$, and z_2 refers to the $1_{-1} \rightarrow 2_{-1}$ transition and is given by $z_2 = 0.15T^{1/2}$.

Finally, we consider vibrational excitation of OH, H₂O, and H₂ by H atoms. At temperatures $T \gtrsim 5000^\circ \text{K}$, where vibrations are readily excited, this loss rate may be comparable to the loss rate due to rotational transitions in the ground vibrational level. For the transition probability, we have employed the semiempirical expression $P(i \rightarrow j) = p_{ij}e^{-p_{ij}}$ (Rapp and Kassal 1969), where p_{ij} is the transition probability as calculated in the limit of small probabilities. $P(i \rightarrow j)$ was averaged numerically over a Maxwellian distribution for the transitions of interest and the resulting probability fitted to a polynomial in T , $P_v(T)$. In calculating the loss rates, we have assumed the same rate dependence as in equation (25). We then find the loss terms ($\text{ergs cm}^{-3} \text{s}^{-1}$)

$$\Lambda_{\text{vib}}(\text{H}_2, \text{H}) = 2.6 \times 10^{-22} T^{1/6} P_{v_1}(T) n_{\text{H}} n(\text{H}_2), \quad (30)$$

$$\Lambda_{\text{vib}}(\text{OH}, \text{H}) = 2.6 \times 10^{-22} T^{1/6} P_{v_1}(T) n_{\text{H}} n(\text{OH}), \quad (31)$$

and

$$\Lambda_{\text{vib}}(\text{H}_2\text{O}, \text{H}) = [3.1 \times 10^{-22} P_{v_1}(T) + 1.4 \times 10^{-22} P_{v_2}(T) + 3.2 \times 10^{-22} P_{v_3}(T)] \\ \times T^{1/6} n_{\text{H}} n(\text{H}_2\text{O}). \quad (32)$$

As mentioned in § II, we have included the heat loss due to thermal dissociation of H₂. It is given by ($\text{ergs cm}^{-3} \text{s}^{-1}$)

$$\Lambda_{\text{diss}}(\text{H}_2, \text{H}) = 1.43 \times 10^{-18} T^{-1/2} e^{-52,000/T} n_{\text{H}} n(\text{H}_2), \quad (33)$$

where we have used the rate constant for the reaction $\text{H}_2 + \text{H} \rightarrow 3\text{H}$ as discussed later in § VI. We have neglected cooling due to collisions between hot atoms and the grains. Only if the atoms can accommodate efficiently at high gas temperatures ($\sim 5000^\circ \text{K}$) could this be an important contribution.

VI. CHEMICAL REACTIONS

We have seen in Paper I that the primary components of the grain mantle are H₂O, CH₄, and NH₃. When the grains are overrun by the shock front, sputtering by He and H atoms will release these species into the gas phase where they will undergo reactions with the atomic and molecular components of the preshock gas. Since the temperature of the gas may now be several thousand degrees, endothermic reactions may occur, in contrast to the reactions that occurred in the preshock phase. However, with the exception of H₂ thermal dissociation, highly endothermic reactions ($\Delta H \approx \text{few eV}$) may generally be excluded, since we will not encounter temperatures $\gtrsim 9000^\circ \text{K}$. All the bimolecular reactions that have been included are listed in table 5. In the cases where the usual preexponential factor of 10^{-10} has been given in rate determinations, we have modified it to the common temperature-dependent factor $2 \times 10^{-11} T^{1/6}$. This value has also been used as the total rate constant for highly exothermic neutral-neutral reactions. Where we have no information on the backward rate k_- , we have used the approximation $k_- \approx k_+ e^{-\Delta H/kT}$, where ΔH is the heat of the reaction. In the two cases of $\text{NH}_3 + \text{H}$ and $\text{CH}_3 + \text{H}$ where no information was available on the activation energies involved, we used Polyani's rule as given by Johnston (1966) to evaluate the activation energy.

Experimental determination of the thermal dissociation rate of hydrogen molecules by hydrogen atoms (Gardiner and Kistiakowski 1961) have yielded an exceptionally high rate, corresponding to a collision diameter of 2.6 Å. Since it is likely that the rate has been overestimated at high temperatures and, furthermore, that dissociation from highly excited vibrational levels has contributed to the overall dissociation rate, we have decreased the preexponential factor by a factor of 10, corresponding to a reason-

able collision diameter of $\approx 1 \text{ \AA}$. The large exponential factor, corresponding to the dissociation energy of H_2 , ensures that this reaction is efficient only for $T \gtrsim 8000^\circ \text{ K}$. Although it is thought that ortho- H_2 and para- H_2 form in their equilibrium ratio of 3:1 (Hollenbach, Werner, and Salpeter 1971), it may be that the ortho-molecules are converted into para-molecules by interaction with the cold grain surfaces (Williams 1970). Conversion back to ortho-molecules may then take place at temperatures $\sim 3000^\circ \text{ K}$. We have included this process using the experimentally determined rate constant given in table 5.

TABLE 5
BIMOLECULAR REACTION RATES

Reaction*	Rate Constants
$A + B \xrightleftharpoons[k_-]{k_+} C + D + \Delta H^\ddagger$	$k_+ (\text{cm}^3 \text{ s}^{-1})$ $k_- (\text{cm}^3 \text{ s}^{-1})$
1. $\text{OH} + \text{H}_2 \rightleftharpoons \text{H}_2\text{O} + \text{H} + 0.69 \text{ eV}$	$6.3 \times 10^{-11} e^{-2240/T} \ddagger$ $4.3 \times 10^{-13} T^{0.68} e^{-9400/T} \S$
2. $\text{OH} + \text{H} \rightleftharpoons \text{H}_2 + \text{O} + 0.09 \text{ eV}$	$9 \times 10^{-12} e^{-3800/T} \ddagger$ $2 \times 10^{-11} e^{-4750/T} \ddagger$
3. $\text{OH} + \text{O} \rightarrow \text{O}_2 + \text{H} + 0.78 \text{ eV}$	$2 \times 10^{-11} T^{1/6} e^{-600/T} \parallel$
4. $\text{OH} + \text{C}^+ \rightarrow \text{CO} + \text{H}^+ + 4.4 \text{ eV}$	10^{-9}
5. $\text{OH} + \text{C} \rightarrow \text{CO} + \text{H} + 4 \text{ eV} \dots$	$2 \times 10^{-11} T^{1/6}$
6. $\text{O} + \text{H} \rightarrow \text{OH} + h\nu \dots \dots \dots$	$3 \times 10^{-16} e^{-3700/T} \#$
7. $\text{CH}_4 + \text{H} \rightleftharpoons \text{CH}_3 + \text{H}_2 + 0.09 \text{ eV}$	$2 \times 10^{-11} T^{1/6} e^{-5900/T} **$ $k_+ e^{-1100/T}$
8. $\text{CH}_3 + \text{OH} \leftarrow \text{CH}_4 + \text{O} + 0.13 \text{ eV} \dots$	$5.3 \times 10^{-11} e^{-4000/T} \ddagger$
9. $\text{CH}_3 + \text{H} \rightleftharpoons \text{CH}_2 + \text{H}_2 + 0.07 \text{ eV}$	$2 \times 10^{-11} T^{1/6} e^{-5600/T}$ $k_+ e^{-800/T}$
10. $\text{CH}_3 + \text{O} \rightarrow \text{CH}_2\text{O} + \text{H} + 1 \text{ eV}$	$2 \times 10^{-11} T^{1/6} \ddagger \ddagger$
11. $\text{CH} + \text{H}_2 \rightleftharpoons \text{CH}_2 + \text{H} + 0.35 \text{ eV}$	$k_- e^{4030/T}$ $5 \times 10^{-13} T^{0.67} e^{-12,850/T} \S$
12. $\text{CH}_2 + \text{O} \rightarrow \text{HCO} + \text{H} + 3.2 \text{ eV}$	$2 \times 10^{-11} T^{1/6}$
13. $\text{CH} + \text{H} \rightleftharpoons \text{C} + \text{H}_2 + 1 \text{ eV} \dots$	$6.7 \times 10^{-11} T^{1/2} e^{-2200/T} \ddagger \ddagger$ $k_+ e^{-11,900/T}$
14. $\text{CH} + \text{C}^+ \rightarrow \text{C}_2^+ + \text{H} + 4.4 \text{ eV}$	10^{-9}
15. $\text{CH} + \text{O} \rightarrow \text{CO} + \text{H} + 7.7 \text{ eV} \dots$	$2.4 \times 10^{-11} T^{1/6}$
16. $\text{CH} + \text{N} \rightarrow \text{CN} + \text{H} + 4.1 \text{ eV} \dots$	$2.4 \times 10^{-11} T^{1/6}$
17. $\text{C} + \text{H} \rightarrow \text{CH} + h\nu \dots \dots \dots$	$10^{-17} [3 - 0.06(T - 20)], 10 \leq T \leq 30^\circ \text{ K}$ $10^{-17} [2.4 - 0.03(T - 30)], 30 \leq T \leq 100^\circ \text{ K}$ $3 \times 10^{-18}, 100 \leq T \leq 200^\circ \text{ K}$ $10^{-18} \text{ if } T \geq 200^\circ \text{ K}$
18. $\text{CH}^+ + e \rightarrow \text{CH} + h\nu \dots \dots \dots$	$5.7 \times 10^{-9} T^{-0.7} \ddagger \ddagger$
19. $\text{C}^+ + \text{H} \rightarrow \text{CH}^+ + h\nu \dots \dots \dots$	$7 \times 10^{-17} \text{ if } T \leq 50^\circ \text{ K}$ $10^{-17} [7 - 0.07(T - 50)], 50 \leq T \leq 100^\circ \text{ K}$ $10^{-17} [7 - 0.015(T - 100)], 100 \leq T \leq 200^\circ \text{ K}$ $10^{-17} \text{ if } T > 200^\circ \text{ K}$
20. $\text{CH}^+ + \text{H} \rightleftharpoons \text{C}^+ + \text{H}_2 + 0.4 \text{ eV}$	$7.5 \times 10^{-15} T^{5/4} \ddagger \ddagger$ $k_+ e^{-4900/T}$
21. $\text{CH}^+ + \text{O} \rightarrow \text{CO} + \text{H}^+ + 4.7 \text{ eV}$	10^{-9}
$\quad \rightarrow \text{CO}^+ + \text{H} + 4.3 \text{ eV}$	10^{-9}
22. $\text{CH}^+ + \text{N} \rightarrow \text{CN} + \text{H}^+ + 1.1 \text{ eV}$	10^{-9}
23. $\text{CH}_2^+ + \text{H} \rightleftharpoons \text{CH}^+ + \text{H}_2 + 0.78 \text{ eV}$	10^{-9} $k_+ e^{-9000/T}$
24. $\text{CH}_2^+ + \text{H}_2 \rightleftharpoons \text{CH}_3^+ + \text{H} + 1.8 \text{ eV}$	10^{-9} $k_+ e^{-21,000/T}$
25. $\text{CH}_4^+ + \text{H} \rightarrow \text{CH}_3^+ + \text{H}_2 + 3.2 \text{ eV}$	10^{-9}
26. $\text{NH}_3 + \text{H} \rightleftharpoons \text{NH}_2 + \text{H}_2 + 0.05 \text{ eV}$	$2.4 \times 10^{-11} T^{1/6} e^{-5700/T}$ $k_+ e^{-600/T}$

(continued)

TABLE 5—Continued

Reaction*	Rate Constants
$A + B \xrightleftharpoons[k_-]{k_+} C + D + \Delta H^\dagger$	k_+ (cm ³ s ⁻¹) k_- (cm ³ s ⁻¹)
27. NH ₂ + H \rightleftharpoons NH + H ₂ + 0.4 eV	$5.8 \times 10^{-14} T^{0.79} e^{-2200/T} \S$ $k_+ e^{-4500/T}$
28. NH + H \rightleftharpoons N + H ₂ + 0.7 eV..	$5 \times 10^{-11} T^{1/2} e^{-2400/T} \S\S$ $k_+ e^{-8300/T}$
29. NH + C ⁺ \rightarrow CN + H ⁺ + 1.5 eV	10^{-9}
30. NH + C \rightarrow CN + H + 3.8 eV..	$2 \times 10^{-11} T^{1/6}$
31. CN + O \rightarrow CO + N + 3.6 eV..	$2 \times 10^{-11} T^{1/6} e^{-1200/T} \ddagger\ddagger$
32. CO ⁺ + H \rightleftharpoons CO + H ⁺ + 0.4 eV	10^{-9} $k_+ e^{-5000/T}$
33. C ⁺ + e \rightarrow C + hν.....	$10^{-11} T^{-1/2} (12.6 - 2.38 \log T) \ \ \ $
34. 3H \leftarrow H ₂ + H + 4.48 eV.....	$2 \times 10^{-7} T^{-1/2} e^{-52,000/T} \#\#\#$
35. H ₂ (para) + H \rightleftharpoons H ₂ (ortho) + H	$2.4 \times 10^{-11} T^{1/6} e^{-3900/T} \ddagger$ $\frac{1}{3} k_+$

* The forward rate constant (k_+) is listed on the first line for a given reaction; the arrow indicates what part of the reaction has been included in the calculations.

† Heats of formation were taken from Nash (1962), bond energies from the *Handbook of Chemistry and Physics* (1964–65), and ionization potentials of the free radicals from Foner (1966). The ionization potential of CH₄ was taken from Marr (1967).

‡ Schofield (1967).

§ Mayer, Schieler, and Johnston (1967).

|| Carroll and Salpeter (1966). Added temperature-dependent preexponential factor.

Solomon (private communication, 1971).

** Kurylo and Timmons (1969); Kurylo, Hollinden, and Timmons (1970). Preexponential factor made temperature dependent.

†† Dean and Kistiakowski (1971). Rate constant made temperature dependent.

‡‡ Klemperer (1971).

§§ Stecher and Williams (1966).

||| Seaton 1955.

Gardiner and Kistiakowski (1961). Preexponential factor reduced by 10.

In table 6 we have listed the nonattenuated photodestruction rates. In the application, these rates have been multiplied with the attenuation factor due to extinction as calculated at the time the shock occurs (Paper I). The rates for the diatomic species were discussed in Paper I. The photodissociation rates of H₂O, CN₄, NH₃, and H₂CO were calculated using the observed absorption cross-sections (as referenced in table 6) together with the radiation field as given by Habing (1968). They agree to within a factor of 2 with the recent, more accurate determinations of Stief *et al.* (1972). In the absence of any experimental information on the absorption cross-sections of the radicals CH₃, CH₂, and NH₂, we assumed the dissociation rates given in table 6. For the photoionization rates, we assumed a constant ionization cross-section between 912 Å and the ionization limit, using the experimental cross-section, or a value of $\sim 10^{-17}$ cm² if no data were available.

The initial H₂/H ratio is a variable-input parameter since the H₂ abundance varies strongly with the position in a cloud due to self-absorption of the ultraviolet photons (Hollenbach *et al.* 1971). In the application, we have considered the two values 10^{-4} and 2×10^{-2} representative for a cloud of $\sim 200 M_\odot$. The corresponding photodestruction rates are given in table 6. Destruction due to low-energy cosmic rays has a rate $\sim 10^{-15}$ s⁻¹ (Solomon and Werner 1971) and may thus be neglected as long as the radiation field is not diluted by more than a factor of 2.5.

TABLE 6
PHOTODESTRUCTION RATES

Reaction $A + \gamma \rightarrow B + C$	Rate Constant k [s ⁻¹]
1. H ₂ O + $\gamma \rightarrow$ OH + H.....	3×10^{-10} *
\rightarrow H ₂ O ⁺ + e.....	0.35×10^{-10} †
2. OH + $\gamma \rightarrow$ O + H.....	4×10^{-12}
\rightarrow OH ⁺ + e.....	1×10^{-12}
3. CH ₄ + $\gamma \rightarrow$ CH ₂ + H ₂	7×10^{-10} ‡
\rightarrow CH ₃ + H.....	1.2×10^{-10} ‡
\rightarrow CH ₄ ⁺ + e.....	5×10^{-11} †
4. CH ₃ + $\gamma \rightarrow$ CH ₂ + H.....	$\sim 5 \times 10^{-10}$
\rightarrow CH ₃ ⁺ + e.....	$\sim 2 \times 10^{-10}$
5. CH ₂ + $\gamma \rightarrow$ CH + H.....	$\sim 5 \times 10^{-10}$
\rightarrow CH ₂ ⁺ + e.....	$\sim 1 \times 10^{-10}$
6. CH + $\gamma \rightarrow$ C + H.....	5×10^{-11}
\rightarrow CH ⁺ + e.....	5×10^{-11}
7. NH ₃ + $\gamma \rightarrow$ NH ₂ + H.....	$\sim 4 \times 10^{-10}$ §
\rightarrow NH ₃ ⁺ + e.....	2.5×10^{-10}
8. NH ₂ + $\gamma \rightarrow$ NH + H.....	$\sim 3 \times 10^{-10}$
\rightarrow NH ₂ ⁺ + e.....	$\sim 1 \times 10^{-10}$
9. NH + $\gamma \rightarrow$ N + H.....	1×10^{-11}
\rightarrow NH ⁺ + e.....	1×10^{-12}
10. CN + $\gamma \rightarrow$ C + N.....	4×10^{-11}
11. CO + $\gamma \rightarrow$ C + O.....	2×10^{-11}
12. CH ₂ O + $\gamma \rightarrow$ CO + H ₂	7×10^{-10} #
2H	
13. CH ₃ ⁺ + $\gamma \rightarrow$ CH ₂ ⁺ + H.....	$\sim 5 \times 10^{-10}$
14. CH ⁺ + $\gamma \rightarrow$ C ⁺ + H.....	3×10^{-12}
15. C + $\gamma \rightarrow$ C ⁺ + e.....	1.4×10^{-10} **
16. H ₂ + $\gamma \rightarrow$ 2H.....	1.0×10^{-11} if H ₂ /H = 10^{-4} ††
	2.5×10^{-14} if H ₂ /H = 2×10^{-2} ††

* Watanabe (1958); 912–1850 Å.

† Wainfan, Walker, and Weissler (1955); Marr 1967.

‡ Wilkinson and Johnston (1950); Sun and Weissler (1955); Magee (1963); 912–1450 Å.

§ Watanabe (1954); Potter and Del Duca (1964); 912–2000 Å.

|| Sun and Weissler (1955).

Gentieu and Mentall (1970); 912–1550 Å.

** Werner (1970).

†† Werner (personal information).

VII. APPLICATION AND RESULTS

We have considered shock waves set up when clouds collide or when they encounter expanding H II regions. We have accordingly studied shock velocities v_1 ($\approx 1/2V$) in the range 5–18 km s⁻¹, spanning the range of the most probable velocities. Assuming no magnetic field or motion along the field lines, a shock wave will occur if v_1 exceeds the sonic speed in the cloud, that is, if $v_1 \geq (5RT_1/3\mu)^{1/2}$. With the same atomic abundances as in Paper I, the molecular weight of the gas is $\mu = 1.27$. He/H has been taken to be 0.09, and the effect of depletion of heavier atoms on μ has been neglected. The preshock density is then $\rho_1 = 2.32 \times 10^{-24} n_H$ (g cm⁻³).

In the preshock phase (Paper I) we treated clouds of 50–1000 M_\odot that evolved under external pressures of 1000 and 1800 cm³ °K. Here we limit ourselves to the case of clouds of 200–500 M_\odot and to an external pressure of 1800 cm³ °K. We chose three representative states of depletion, $d(C^+) = 0.89, 0.19, \text{ and } 0.028$. The first value

corresponds to a cloud with an “age” about equal to the average cloud-cloud collision time of 10^7 years (“epoch 1”); the second value corresponds to a more evolved cloud ($\sim 4 \times 10^7$ years, “epoch 2”); and the last value denotes an “old” cloud ($\sim 10^8$ years, “epoch 3”). For the latter we considered only one strong shock of $v_1 = 18 \text{ km s}^{-1}$.

To integrate the 29 dependent variables through the cooling region, we employed a computer adaption of the Zonnefeld-Adams-Moulton solution of differential equations. The time derivative of the concentration of species i relative to H, $c_i \equiv n_i/n_H$, was calculated via $dc_i/dt = \beta_i/n_H - \alpha_i c_i$, with β_i and $\alpha_i n_i$ being the total formation and destruction rates ($\text{cm}^{-3} \text{ s}^{-1}$), respectively. However, because of the problem of stiffness in these equations, whenever the timescales for changes in the formation and/or destruction rates were sufficiently long, we resorted to analytical approximations to the change in the variable for a given step size. In addition, we “dropped” variables when their concentration became less than 10^{-18} .

We divided the grain into two components, the “CH₄ grain,” which is composed solely of CH₄, and the “H₂O grain,” which is composed of all the other species (Paper I). We assumed the sputtering rate of a given species other than H₂O and CH₄ to be equal to the sputtering rate of H₂O multiplied by its relative abundance in the mantle. The decrease in the radii is then given by $da_{\text{CH}_4}/dt = -M_{\text{CH}_4}/(4\pi a_{\text{CH}_4}^2 \rho_g) \times [S_{\text{H}}(\text{CH}_4) + S_{\text{He}}(\text{CH}_4)]$, and $da_{\text{H}_2\text{O}}/dt = -M_{\text{H}_2\text{O}}/(4\pi a_{\text{H}_2\text{O}}^2 \rho_g)(b_M/b_t)S_{\text{H}}(\text{H}_2\text{O})$. Here ρ_g is the density in the mantle (1.5 g cm^{-3}), $b_M = \sum b_i M_i/M_{\text{H}_2\text{O}}$, and $b_t = \sum b_i$, where b_i is the abundance of species i in the mantle relative to H₂O, M_i being its mass. The summations are over all the species in the H₂O grain. The sputtering was considered to be complete for either grain when the radius was equal to the core radius $a_0 = 0.05 \mu$. The actual grain radius was calculated via $a^3 = a_{\text{H}_2\text{O}}^3 + a_{\text{CH}_4}^3 - a_0^3$. Except for CH₄, the formation rate of species i in the gas phase due to sputtering is given by $\beta_s(i) = (b_i/b_t)S_{\text{H}}(\text{H}_2\text{O})n_{\text{gu}}/v$, while for CH₄ we have $\beta_s(\text{CH}_4) = [S_{\text{H}}(\text{CH}_4) + S_{\text{He}}(\text{CH}_4)]n_{\text{gu}}/v$.

In calculating the radiative loss rates, we took account of the depletion of the cooling elements as well as their gradual return to the gas phase. The criterion for ending the calculation was that the heat loss be within a factor of 2 of the heat gain due to cosmic-ray ionization as given by Penston (1970). However, since we neglected resumed depletion in the postshock phase, we did not continue the calculation if the cooling time τ_{cool} became too large to satisfy the relation $\tau_{\text{cool}}n_{\text{H}} \lesssim 10^8 \text{ years cm}^{-3}$.

Figure 1 shows typical temperature and density profiles behind the shock front. For shock velocities 5–18 km s^{-1} we see that the time it takes for the gas to cool down to $\sim 10^\circ \text{ K}$ is generally about 10^4 years. More than two-thirds of this time is spent with cooling from 100° to 10° K . For temperatures $\lesssim 25^\circ \text{ K}$, we find that the neutral carbon lines dominate the cooling rate by more than 60 percent.

From the curve for a shock velocity of 10 km s^{-1} , we see that by increasing the H₂ abundance from 10^{-4} to 2×10^{-2} , the cooling time decreases by about 10^3 years. However, for a shock velocity of 18 km s^{-1} we find that there is essentially no decrease in the cooling time when the H₂ abundance is high. At such high shock speeds the temperature is high enough ($\geq 8000^\circ \text{ K}$) so that thermal dissociation of H₂ by H atoms is important. We find that when $v_1 = 18 \text{ km s}^{-1}$, the molecular hydrogen abundance is decreased from 2×10^{-2} to $\sim 10^{-5}$ in about 150 years, which is much shorter than the timescale for cooling.

In figure 2 we show the variation with time for all the chemical species behind the shock front that attain an abundance of 10^{-7} or more with respect to atomic hydrogen. We see that the variation of the abundances of CH₄, CH₃, CH₃⁺, CH₂, and CH⁺ is extremely rapid and that these species are abundant only within $\sim 10^2$ years of the shock front, corresponding to a distance of about $3 \times 10^{-4} \text{ pc}$ from the shock front. These molecules are being created very rapidly by the rapid sputtering of the CH₄ grain, but they are also being destroyed very fast through abstraction reactions with H atoms.

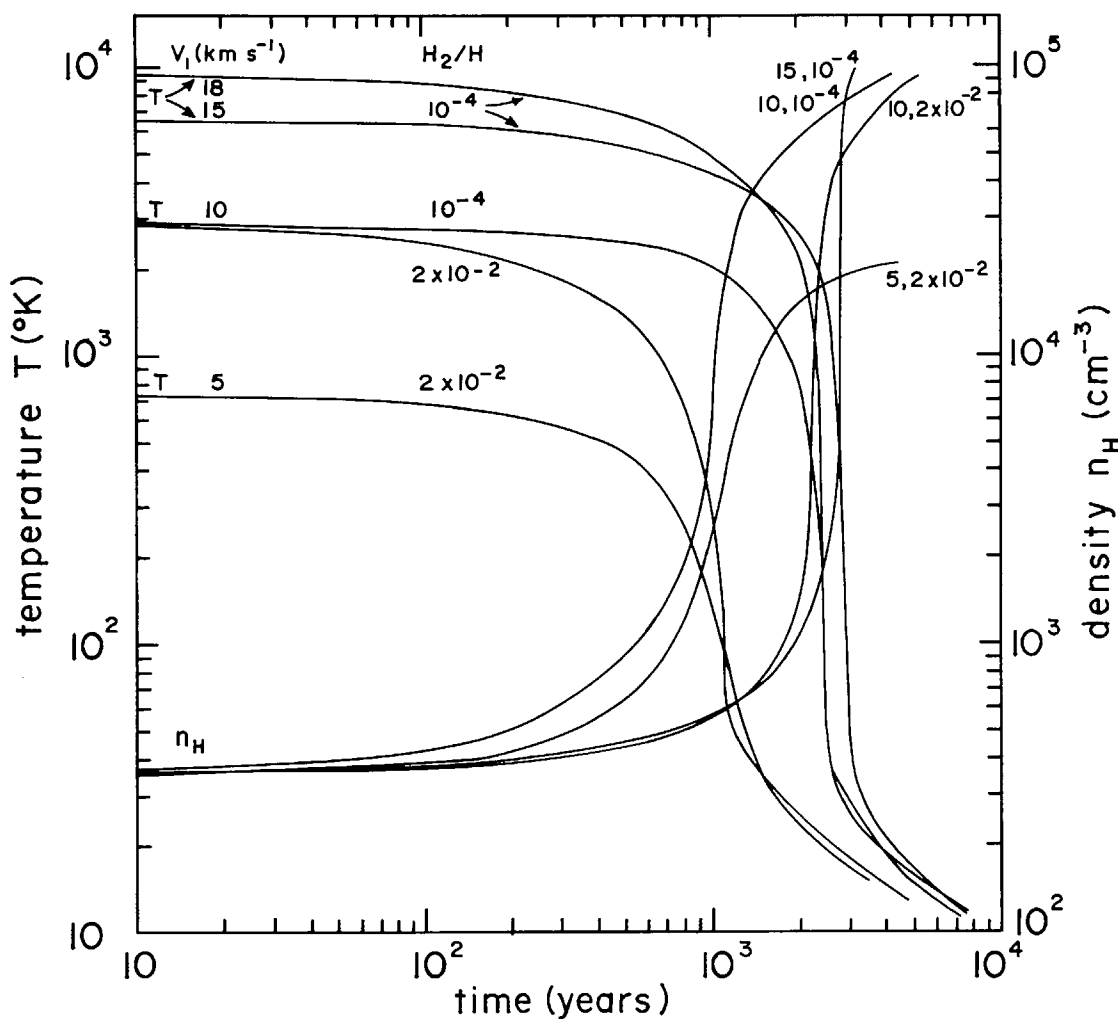


FIG. 1.—Postshock temperatures and densities as functions of the time since a gas element passed through the shock front. The shock velocities v_1 and the relative molecular hydrogen abundances H_2/H are indicated in the upper left for the temperature profiles and in the upper right for the density profiles. For the 18 km s^{-1} shock velocity, only the temperature profile is shown. The preshock gas has a depletion factor $d(C^+) = 0.89$, and the cloud mass is $200 M_\odot$.

OH and H_2O are abundant over a much larger range, corresponding to $\sim 10^3$ years from the shock front (or 10^{-3} pc in distance from the front). However, as the gas cools below 10^3 K, the main formation mechanisms become ineffective (sputtering for H_2O and the reaction $H_2 + O \rightarrow OH + H$ for OH) and the abundances fall rapidly. For such temperatures, the most important formation mechanism for OH is photodissociation of H_2O . However, this rate is never large since the abundance of H_2O becomes small and is rapidly decreasing when $T < 10^3$ K. We also see that high initial temperatures (*dashed curves*) actually decrease the H_2O abundance in most of the shock wave. This is due to the reaction $H_2O + H \rightarrow OH + H_2$, which is rapid at high temperatures. However, when the temperature drops to about 4000°K , this destruction mechanism becomes less effective and the H_2O abundance rises rapidly due to the backward reaction which has a much smaller activation energy. H_2O/H finally reaches a maximum of 3×10^{-6} at a temperature of $\sim 1000^\circ \text{K}$ and density of $\sim 2400 \text{ cm}^{-3}$. In the latter phases H_2O is destroyed mainly through photodestruction processes. OH, on the other hand, is destroyed more rapidly than H_2O through the

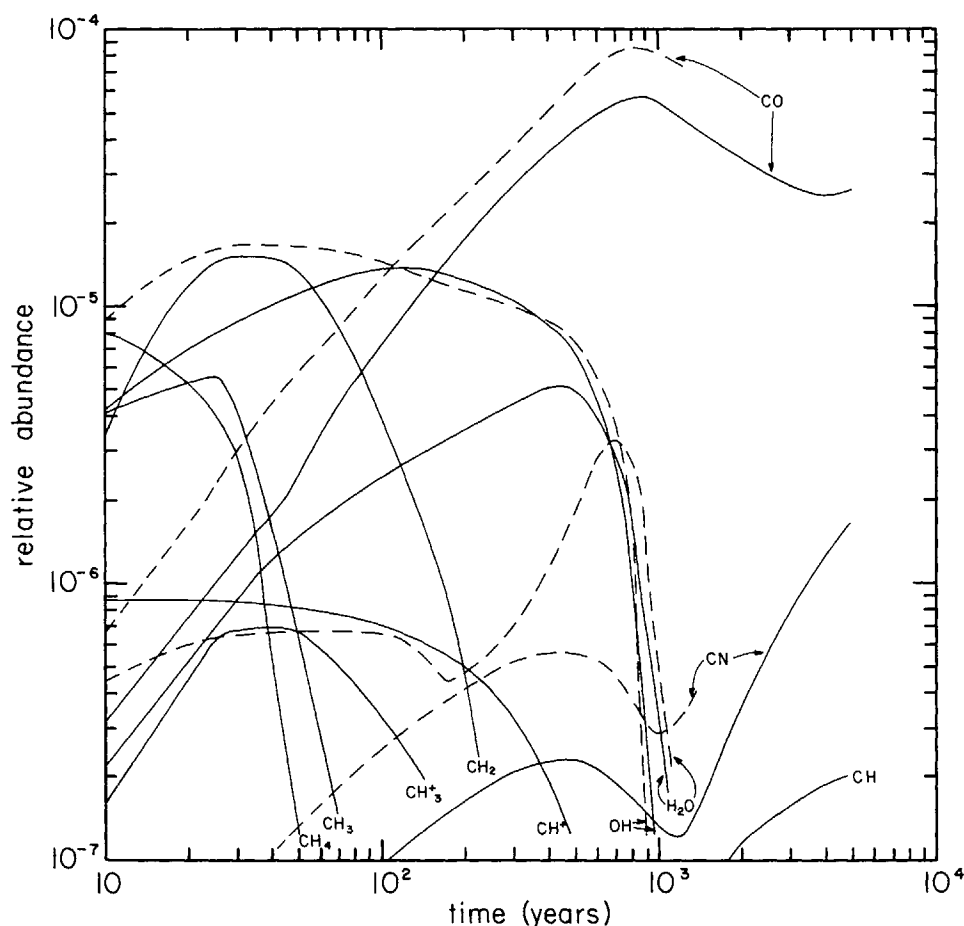


FIG. 2.—Molecular abundances relative to atomic hydrogen as functions of time. *Solid curves*, for an abundance $H_2/H = 2 \times 10^{-2}$ and a shock velocity $v_1 = 10 \text{ km s}^{-1}$. *Dashed curves*, for the same H_2 abundance but with a shock velocity of 15 km s^{-1} . Preshock state as in fig. 1.

reaction $OH + C^+ \rightarrow CO + H^+$, so that H_2O is somewhat more abundant than OH in the end.

From figure 2 we see that the most abundant molecule is CO , except in the early parts of the shock wave. CO “feeds” on the amount of OH through the reaction given above and is destroyed mainly by the relatively slow photodestruction. CO reaches a maximum abundance of $\sim(6-8) \times 10^{-5}$ at about 10^3 years from the shock front ($T \approx 300^\circ \text{ K}$, $n_H \sim 600 \text{ cm}^{-3}$) and then slowly decreases due to photodestruction. However, in the very cold ($T \lesssim 30^\circ \text{ K}$) and dense ($n_H \gtrsim 2000 \text{ cm}^{-3}$) region, the abundance of CO levels off to $\sim 2.5 \times 10^{-5}$, due to the reaction $CH + O \rightarrow CO + H$, which becomes important when the density is high and the temperature is low so that CH is formed effectively through radiative association. It is this process that limits the abundance of CH to $\sim 2 \times 10^{-7}$ in the dense postshock region. CH also reacts to form CN very effectively in this region, causing the CN abundance to increase rapidly for densities $\gtrsim 10^3 \text{ cm}^{-3}$. In the final state ($T \approx 10^\circ \text{ K}$, $n_H \approx 8 \times 10^4 \text{ cm}^{-3}$) the only molecules of any importance are seen to be CO , CN , and CH , decreasing in abundance by roughly an order of magnitude in the order listed. For these molecules, formation and destruction rates are approximately in balance and their abundances will characterize the whole region of a cloud traversed by the shock front.

The same final state is obtained if the initial H_2 abundance is decreased to $H_2/H = 10^{-4}$. This is shown in figure 3. However, both the OH and H_2O abundances are now

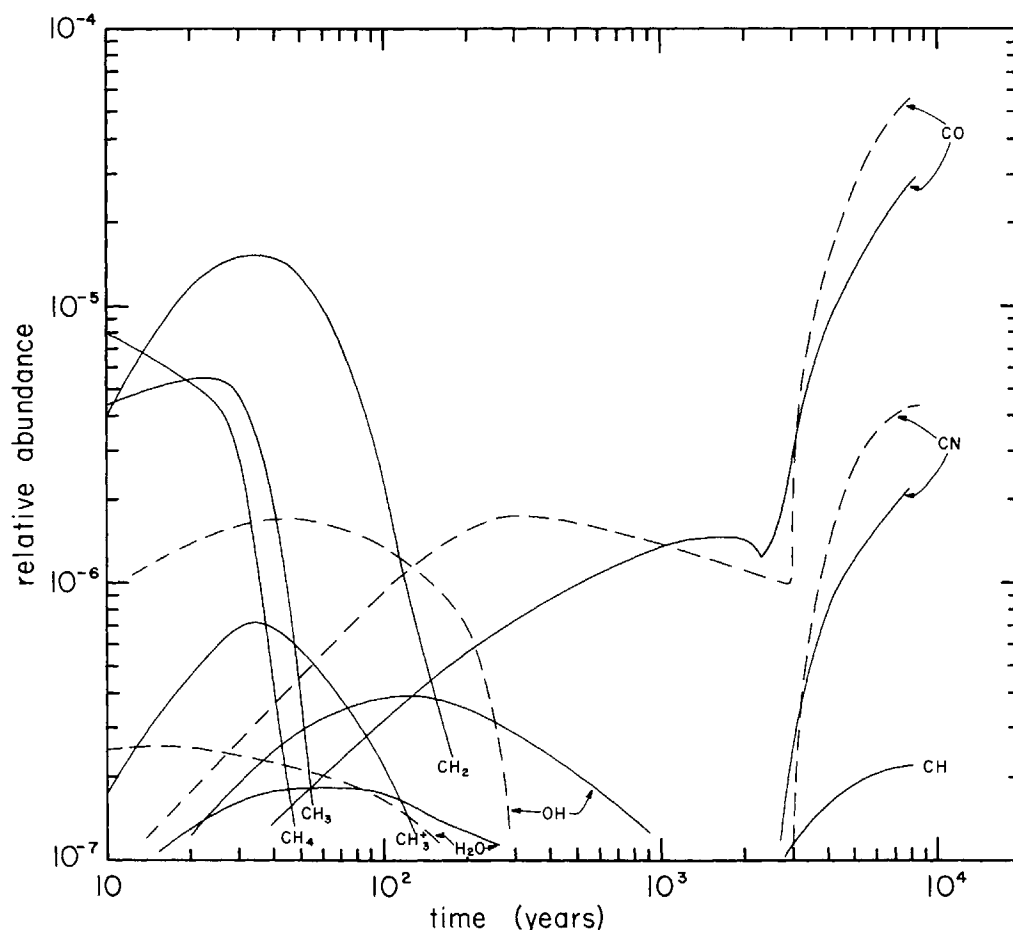


FIG. 3.—Molecular abundances relative to atomic hydrogen as functions of time. *Solid curves*, for an abundance $H_2/H = 10^{-4}$ and a shock velocity $v_1 = 10 \text{ km s}^{-1}$. *Dashed curves*, for the same H_2 abundance but with a shock velocity of 15 km s^{-1} . The preshock state is as in fig. 1.

generally smaller than in figure 2, being $\leq 10^{-6}$. This reflects the importance of the reactions $O + H_2 \rightarrow OH + H$ and $OH + H_2 \rightarrow H_2O + H$ for forming OH and H_2O . We also see that the increase in shock velocity from 10 to 15 km s^{-1} increases the abundances of OH and H_2O much more than was the case in figure 2. This is because the sputtering of the H_2O grain is now the main source for OH and H_2O and a shock velocity of 10 km s^{-1} is not quite able to “clean” the grain, while a 15 km s^{-1} shock velocity destroys the mantle in ~ 250 years (see fig. 6).

However, when the H_2 abundance is small, sputtering will clearly be most important as a source of H_2O and OH when the grains have large mantles. In figure 4 we show the abundances of H_2O and OH behind the shock front for preshock gas in epochs 2 and 3, when the grain radii are 0.14 and 0.16μ , respectively. We see that these two cases give about the same amounts of OH and H_2O as we had in figure 2 with much smaller grains and the higher H_2 abundance.

In figure 5 we show how the column densities of OH and H_2O vary with the shock velocity. We see that in both cases the column density reaches a maximum and then decreases with increasing velocity. This is because the highest temperatures lead to rapid hydrogen abstraction reactions as well as thermal dissociation of H_2 , so that the backward reactions are small. We also see that similar column densities, $\geq 10^{13} \text{ cm}^{-2}$, are obtained either when H_2 is abundant ($H_2/H = 2 \times 10^{-2}$) or when the grain mantles are large [$d(C^+) \leq 0.2$] and subsequently sputter down for large shock

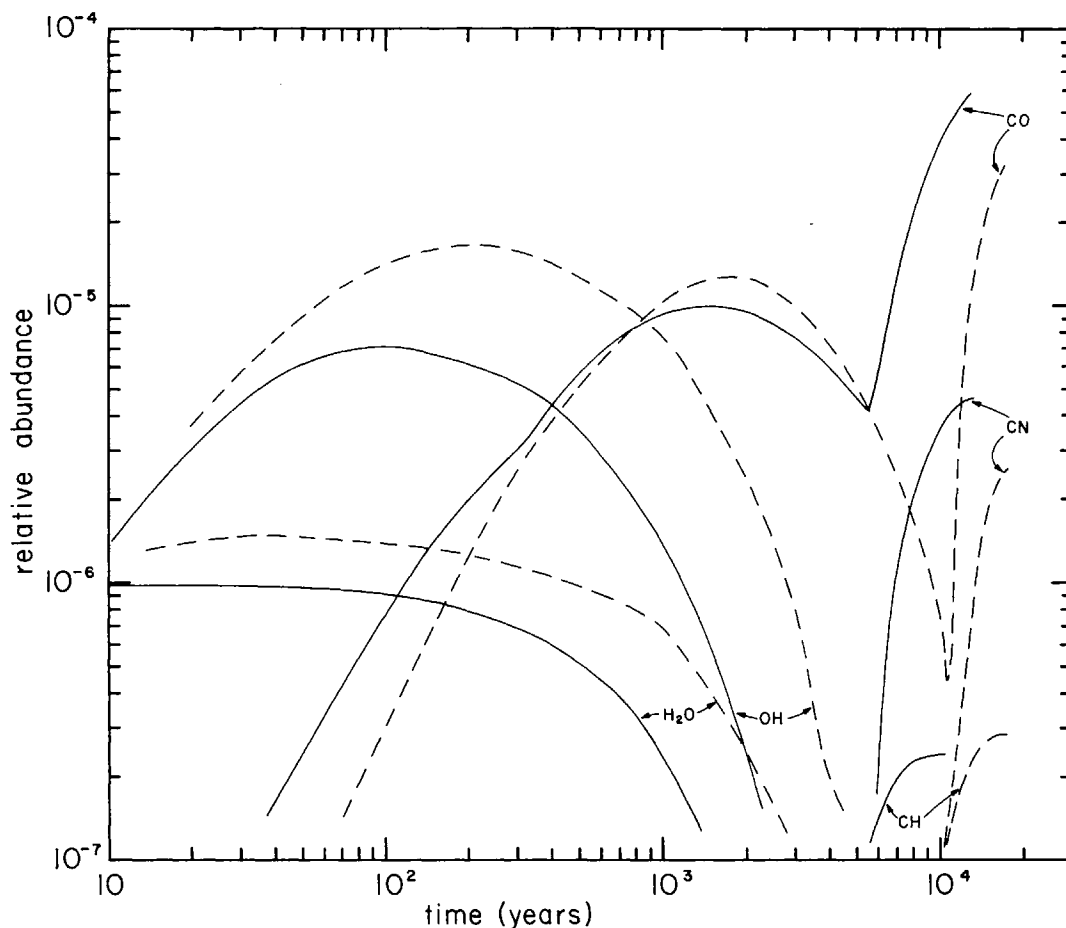


FIG. 4.—Molecular abundances relative to atomic hydrogen as functions of time. *Solid curves*, for preshock gas with depletion factor $d(C^+) = 0.19$ and a shock velocity of 15 km s^{-1} . The cloud mass is $200 M_{\odot}$. *Dashed curves*, for preshock gas with depletion factor $d(C^+) = 0.028$ and a shock velocity of 18 km s^{-1} . The cloud mass is $500 M_{\odot}$. The initial H_2 abundance is $\text{H}_2/\text{H} = 10^{-4}$ for both sets of curves.

velocities. The column densities of CO, CN, and CH are from 10^{13} to 10^{14} cm^{-2} through the shock wave. However, since these species are in approximate equilibrium in the dense and cold region, their actual column densities are larger and depend upon how much of the cloud has been traversed by the shock front.

As mentioned above, we also studied the conversion of para-hydrogen into ortho-hydrogen. With an arbitrary initial para/ortho ratio of 99 and a shock velocity of 10 km s^{-1} , the equilibrium ratio of 1/3 was established in about 10 years from the shock front. This process thus seems very efficient for typical cloud velocities.

In figure 6 we show how the velocity of the grain with respect to the gas and the radius of the grain vary behind the shock front. We see that the grain is effectively stopped (velocity $< 1 \text{ km s}^{-1}$) only in the very dense and cold regions far behind the shock front. It thus reaches a distance of from 10^{-3} to 10^{-2} pc from the shock front, depending on the shock velocity. We also see that the higher H_2 abundance leads to a slightly higher relative velocity between gas and grains. This is due to the fact that the gas cools faster when H_2 is abundant, so that it becomes denser and the gas flow velocity becomes correspondingly smaller.

We see that a small-grain mantle (epoch 1) is not sputtered completely down for a shock velocity of 10 km s^{-1} but that a velocity of 15 km s^{-1} is quite effective in this

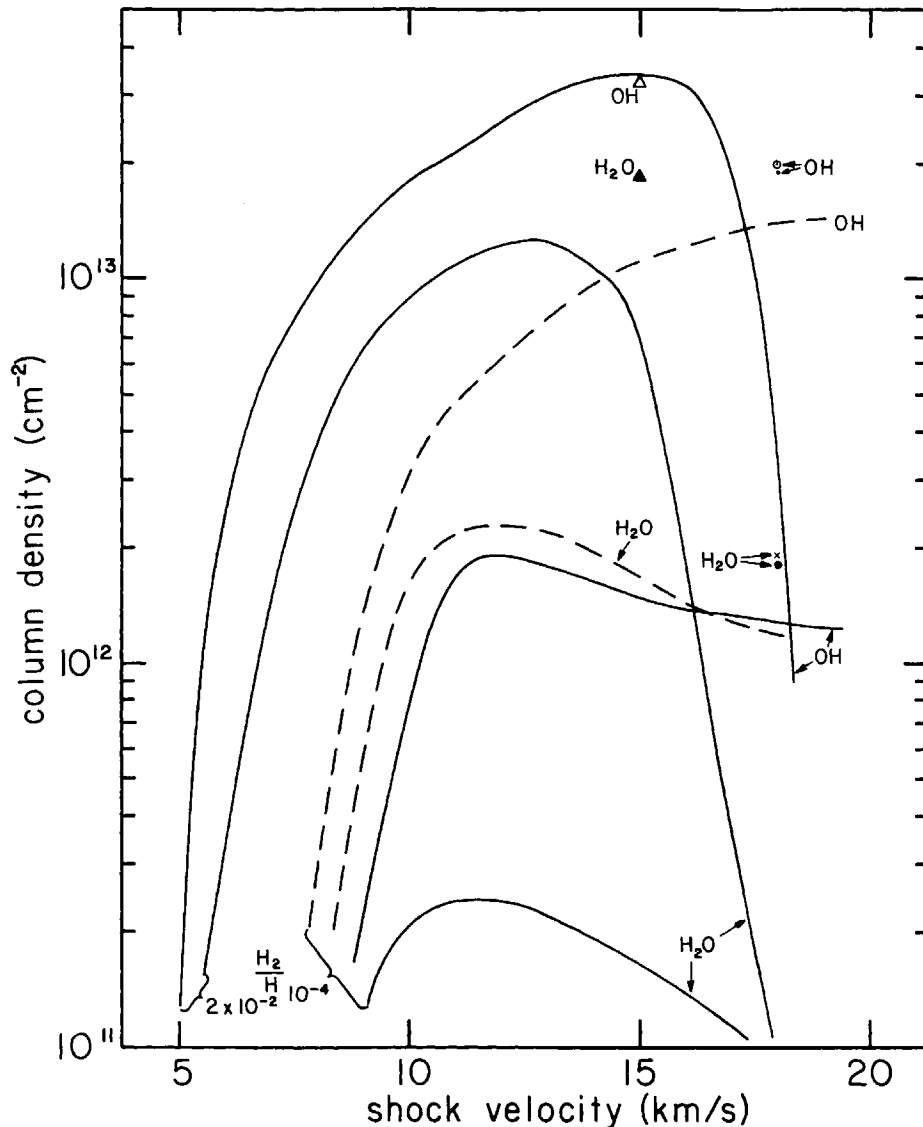


FIG. 5.—Column densities of OH and H₂O in the shock wave as functions of the shock velocity. *Solid curves*, for a cloud of 200 M_{\odot} with an initial depletion factor $d(C^+) = 0.89$. *Dashed curves*, for a cloud of 500 M_{\odot} with an initial depletion factor $d(C^+) = 0.19$. H₂ abundance is as indicated. The points are for cases where only one shock velocity was studied. Solid and open triangles correspond to parameters as for the dashed curves but with $H_2/H = 2 \times 10^{-2}$. The two pairs of symbols (\cdot , \times) and (\odot , \bullet) correspond to a cloud of 500 M_{\odot} with an initial depletion factor of 0.028 and H₂ abundances of 2×10^{-2} and 10^{-4} , respectively.

respect. For a large grain (epoch 2, *dashed curves*), a shock velocity of 15 km s^{-1} is not quite adequate to sputter the mantle down if $H_2/H = 10^{-4}$, but with an H₂ abundance of 2×10^{-2} the process is quite effective and the grain mantle is destroyed in about 10^3 years. This difference is due to the extra-rapid cooling when H₂ is large, causing the relative velocity between grains and gas to remain high as discussed above.

In figure 7 we show how the final grain radius depends on the shock velocity. The dashed parts of the curves are extrapolations where we have taken into account that even small shock velocities ($\lesssim 5 \text{ km s}^{-1}$) will probably be able to sputter the CH₄ grain, mainly due to the velocity difference of a few km s^{-1} between grains and gas (see tables 2 and 3). The points in figure 7 are for cases where we studied only one

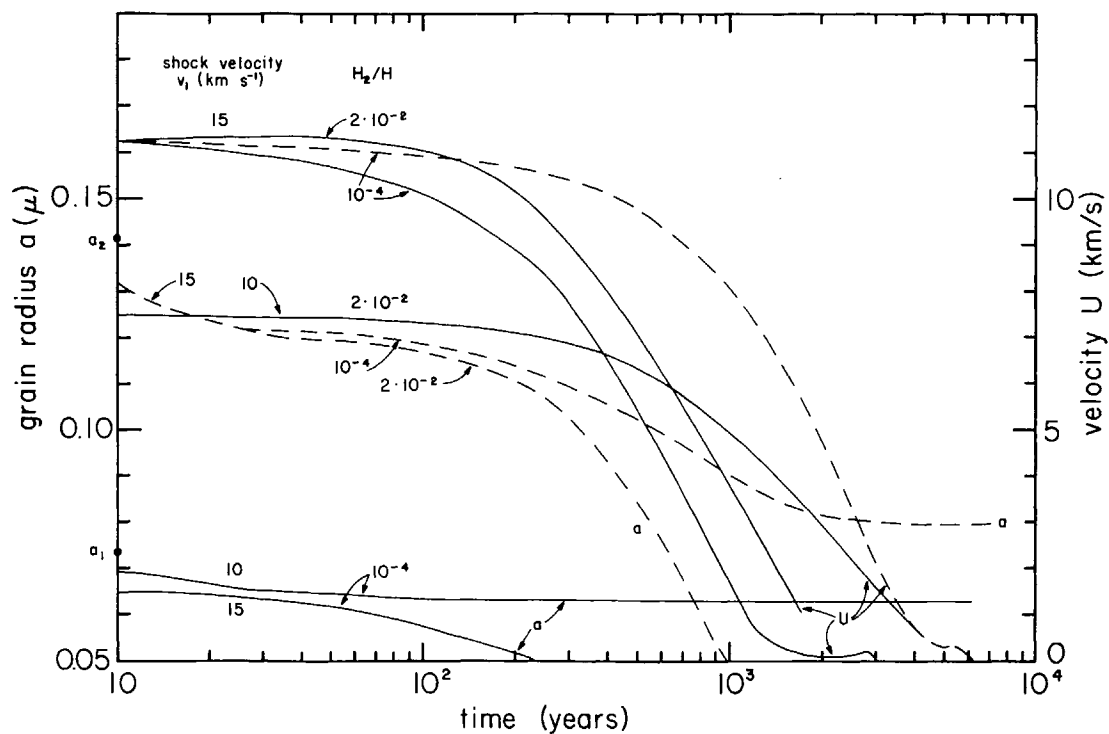


FIG. 6.—Relative velocity between grain and gas and the grain radius as functions of time. *Solid curves*, for preshock gas with parameters as in fig. 1 (epoch 1). *Dashed curves*, for preshock gas with a depletion factor $d(C^+) = 0.19$ (epoch 2). The initial grain radii are denoted by a_1 and a_2 , respectively.

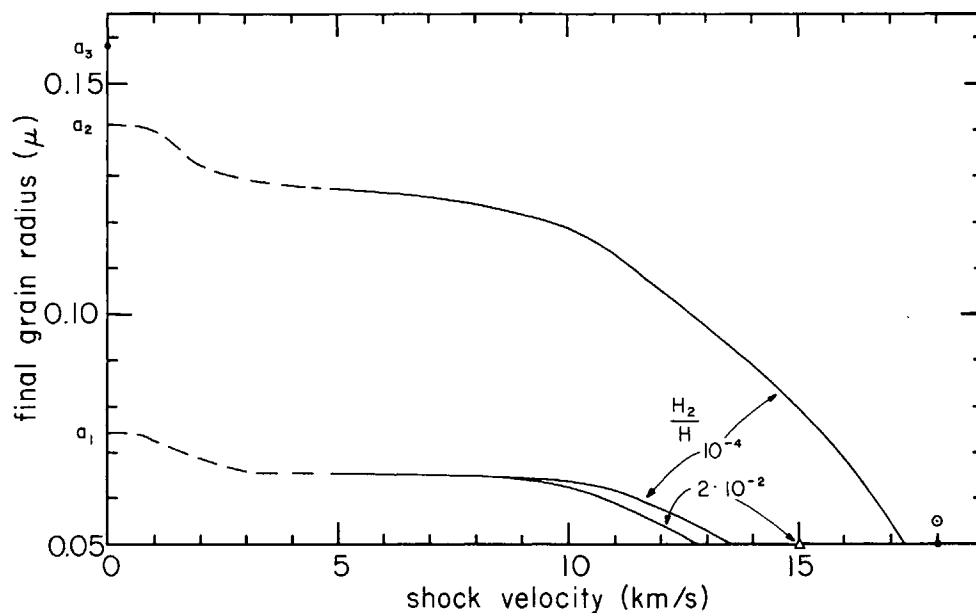


FIG. 7.—Final grain radii as functions of the shock velocity. *Lower curve*, for gas with initial depletion factor $d(C^+) = 0.89$; *upper curve*, for $d(C^+) = 0.19$. Molecular hydrogen abundances as indicated. Open triangle denotes the final radius for $d(C^+) = 0.19$ and $H_2/H = 2 \times 10^{-2}$. The symbols \odot and \bullet are for an initial depletion factor $d(C^+) = 0.028$ and H_2 abundances of 10^{-4} and 2×10^{-2} , respectively. Initial radius for this case (epoch 3) denoted as a_3 .

shock velocity. We see that a large mantle is sputtered down only when the shock velocities $\geq 15 \text{ km s}^{-1}$, but we again note that a high H_2 abundance increases the efficiency of the sputtering process substantially.

In figure 8 we show the most important radiative fluxes from a shock wave as a function of the shock velocity. We see that the fluxes from the rotational lines of H_2 are sharply decreased as the shock velocity becomes greater than about 15 km s^{-1} . This is due to the importance of thermal dissociation of H_2 . We also see that the added cooling lines of O^0 (6300 \AA), Fe^+ (4.1μ), and Fe^+ (5.4μ) are important, especially at velocities $\geq 15 \text{ km s}^{-1}$. At temperatures $\geq 7500^\circ \text{ K}$, the 6300 \AA line carries more than 80 percent of the total radiated energy.

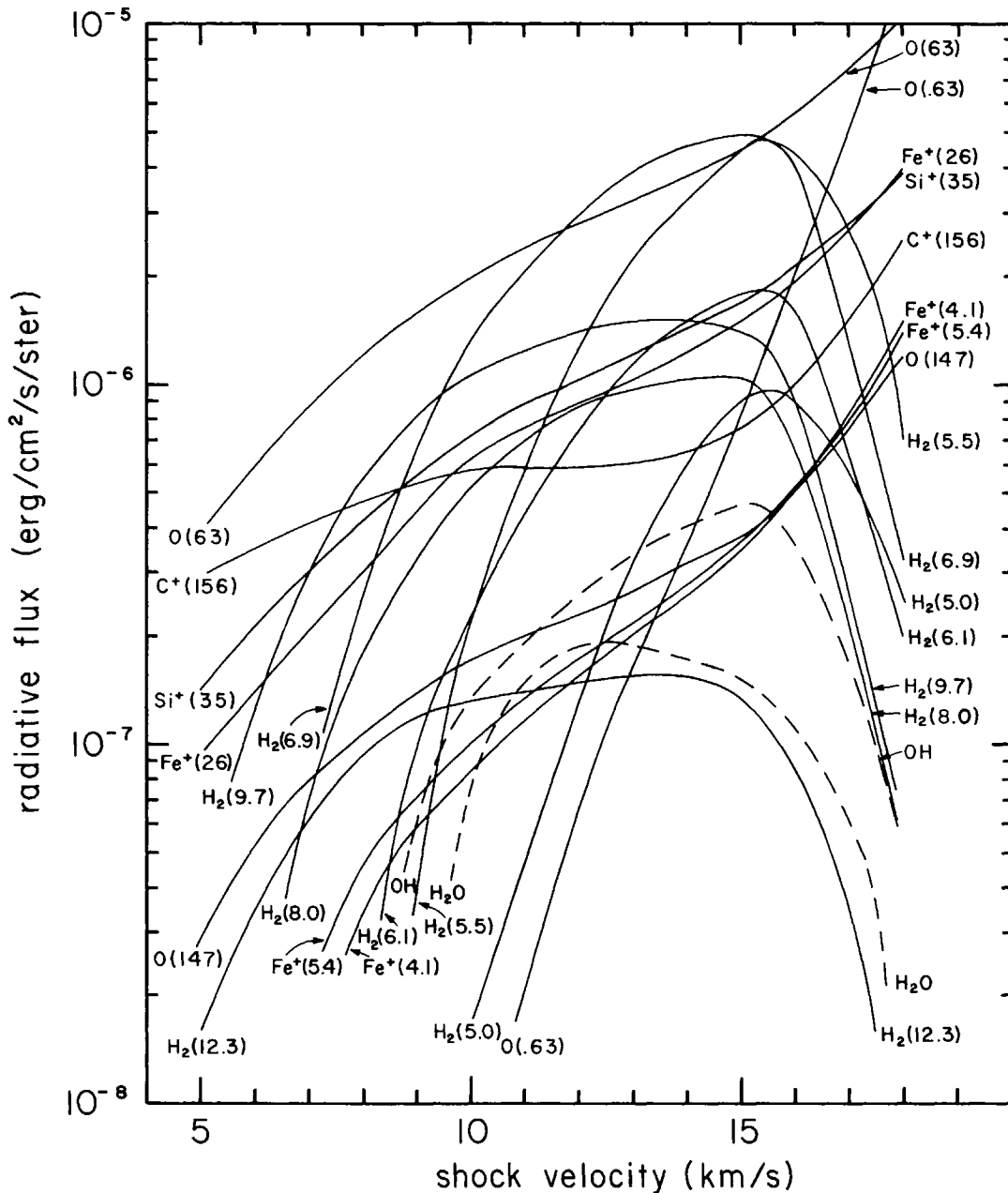


FIG. 8.—Radiative fluxes from a shock wave as functions of the shock velocity. The cooling elements and the transition wavelength in microns are indicated on both sides of the graph. The state of the preshock gas is as in fig. 1 and $\text{H}_2/\text{H} = 2 \times 10^{-2}$.

The total fluxes in the rotational transitions of OH and H₂O (H atom and electron excitation) are indicated by the dashed lines. They are generally about an order of magnitude smaller than the most important radiative fluxes. We found that the fluxes due to the vibrational transitions of OH and H₂O as well as H₂ were small relative to the fluxes from the rotational transitions (≤ 0.01), even at the highest shock velocities.

VIII. DISCUSSION

For typical shock velocities we have found that interstellar clouds may cool down to about 10° K in a time slightly less than 10⁴ years. The times for cooling to about 100° K are even shorter than those found by FRAO by a factor of 3–4. This is due mainly to somewhat higher preshock densities and, to a smaller extent, to the inclusion of more cooling processes. The gas spends most of the 10⁴ years in cooling below 100° K, and at $\sim 10^\circ$ K the energy loss rate is usually within a factor of 2 of the cosmic-ray heating rate of $\sim 10^{-21}$ erg cm⁻³ s⁻¹.

However, we see that the gas will probably cool even a little below 10° K if rotational cooling by the abundant CO molecule (figs. 2–4) is included. The lowest rotational transition in CO is $\sim 5^\circ$ K, and if we assume a collision radius with H atoms of 1.5 Å, the loss rate at $T \approx 10^\circ$ K and $n_{\text{H}} \approx 10^5$ cm⁻³ from the excitation of the ($J = 1$) level alone would be $\Lambda_{\text{H}}(\text{CO}) \approx 3 \times 10^{-21}$ erg cm⁻³ s⁻¹, which may be compared with the loss rate due to the neutral carbon lines of $\sim 2 \times 10^{-21}$ erg cm⁻³ s⁻¹ for the same conditions. Thus, it appears that rotational cooling by CO may cool the gas further from 10° to $\sim 5^\circ$ K.

The large abundance of CO far behind the shock front is of importance, since recent results (Penzias, Jefferts, and Wilson 1971) indicate that CO is very abundant near interstellar H II regions, having column densities $\sim 10^{19}$ cm⁻². From figures 2–4 we see that the equilibrium abundance of CO in the dense region may be $\sim 10^{-4}$ for typical shock velocities expected outside H II regions (≥ 14 km s⁻¹). However, the maximum column densities for the clouds considered here would be $\sim 10^{17}$ cm⁻², and the observations must therefore refer to much more massive clouds.

Münch (1964) presented evidence that a high concentration of CN molecules exists in an interstellar cloud in the immediate neighborhood of the H II region near the cluster NGC 7822. The column density is about 3×10^{14} cm⁻², and the ratio of CN to CH is about 2. Münch suggested that the CN molecules were formed in the dust grains of the H I region when flashed by the ultraviolet radiation in the advancing ionization front. On the basis of the calculations here, however, we suggest that the anomalous CN abundance arises by gas-phase reactions in the cold and dense region behind the shock front that precedes the ionization front. Similarly, this could be the explanation for the anomalous abundance of CN found in 20 Aql (Frisch 1972).

In contrast to the species CO and CN which may be formed efficiently throughout the compression region, OH is formed only in the hot region immediately behind the shock front. However, the sputtering process is inherently inefficient for forming OH, since the high temperatures also destroy OH rapidly via the reaction $\text{OH} + \text{H} \rightarrow \text{H}_2 + \text{O}$. Only if H₂ is abundant, $\sim 10^{-2}$ relative to H, is the backward reaction important for forming OH, and it will then in general dominate the previous rate for formation of OH. Since very large shock velocities destroy H₂ via thermal dissociation by H atoms, the largest OH abundance in a shock wave will be obtained for average cloud velocities, $v_1 \approx 10$ km s⁻¹. From figure 5 we see that the largest column densities of OH are $N_{\text{OH}} \sim 10^{13}$ cm⁻².

Since the densities behind the shock front are high enough (> 200 cm⁻³) for the excitation temperature T_s to be effectively coupled to the kinetic temperature (Goss 1967), which is $\geq 10^3$ ° K, OH may appear more often in emission than in absorption. Many of the background sources observed by Goss are H II regions, so that only if the

optical depth $\tau \gtrsim 0.1$ would we expect to see the hot OH in absorption. Only few sources satisfy this condition. Furthermore, even for sources where we would expect absorption, the observed value $N_{\text{OH}}/T_s \approx 10^{13} \text{ cm}^{-2} (\text{deg-K})^{-1}$ (Goss 1967) gives a column density $N_{\text{OH}} \approx 10^{16} \text{ cm}^{-2}$, which is larger than the computed value by a factor of 10^3 . We conclude that a model of hot OH in absorption can probably not account for the observations unless the clouds are much more massive than the ones treated here.

Since we have neglected any formation of OH in the dense, postshock region, we may consider the possibility that the observed OH (in absorption) is located within this region. With the main destruction mechanism in this region, $\text{OH} + \text{C} \rightarrow \text{CO} + \text{H}$, we find that the preassociation mechanism (Julienne, Krauss, and Donn 1971) fails by four orders of magnitude to explain the observed value $\text{OH}/\text{H} \approx 10^{-7}$. Catalytic surface reactions as employed in Paper I fail by one order of magnitude. We conclude that formation of OH in quiescent clouds (Paper I) where OH is formed on the grains but destroyed via photodissociation can best explain the observations of OH in absorption.

We noted above that hot OH may appear in emission against H II regions. Without attempting to explain the many anomalous features of OH line emission, we note that the total column density of OH through the shock front (fig. 5) would produce an antenna temperature (in the optically thin case and for the 1667-MHz transition) $\Delta T \approx 1^\circ \text{ K}$. In several cases an OH emission line of $\Delta T \approx 1^\circ \text{ K}$ is observed with a velocity $\sim 10 \text{ km s}^{-1}$ less than the absorption line (Weaver *et al.* 1965). The absorption may originate in the part of a cloud where OH is formed in the quiescent phase. The hot OH behind the shock front may cause the emission and will typically have a velocity $-(v_1 - v_1 \rho_1 / \rho_2) \approx -10 \text{ km s}^{-1}$ with respect to the material ahead of the shock. However, as discussed by Goss (1967), the relation between the OH emission and absorption velocities may be just kinematical and not physical.

We now consider the destruction of the grain mantle. We see from figure 7 that the critical shock velocity for complete removal of the grain mantle is not a very sensitive function of the initial grain radius, especially for the higher H_2 abundance. For grain radii $0.05\text{--}0.14 \mu$ and assuming $\text{H}_2/\text{H} \approx 10^{-2}$ or greater, we may take $v_{1,\text{crit}} = 13\text{--}15 \text{ km s}^{-1}$. Thus, the probability of mantle removal is equal to the probability of two clouds colliding with a relative velocity $V \gtrsim 25\text{--}30 \text{ km s}^{-1}$. Using the expression given by Kahn (1955) and a velocity dispersion for clouds of 8 km s^{-1} (Spitzer 1968), we find that this probability is $0.3\text{--}0.1$. Since the collision frequency between interstellar clouds is $\sim (7 \times 10^6 \text{ years})^{-1}$, we obtain a destruction probability per unit time of about $(4.3\text{--}1.4) \times 10^{-8} \text{ year}^{-1}$. We conclude that mantles may be effectively destroyed in cloud-cloud collisions every 5×10^7 years if the molecular hydrogen abundance is not much less than 1 percent.

With a rate of grain growth $\sim 10^{-13} \text{ cm year}^{-1}$ (Paper I), we find the steady-state distribution of grain radii to be $n(a)/n(a_0) = e^{-20(a-a_0)}$, where a is the grain radius in microns and a_0 is the core radius (0.05μ). Using this distribution function, the average grain radius for core-mantle grains is found to be $\bar{a} = 0.1\text{--}0.07 \mu$. Attempts to observe absorption bands of ice in interstellar grains would set a limit on the average mantle size $\bar{a} \lesssim 0.06 \mu$ if the mantle has ice in it. Since correction for circumstellar extinction may increase this limit, the discrepancy may not be serious. On the other hand, a large sputtering efficiency depends on the molecular hydrogen abundance being at least 1 percent. Furthermore, grain growth in the dense, postshock region may take place on a timescale 10^3 times smaller than in the preshock phase, increasing the rate of grain growth accordingly. Such rapid growth should be taken into account in future investigations of equilibrium size distributions.

Oort and van de Hulst (1946) considered grain-grain collisions as a mechanism for the destruction of interstellar grains. From our calculations we find that the size of the

region where such collision may take place is about 1.2×10^{-3} pc, corresponding to 10 percent of the total mass of the type of clouds we consider here. Furthermore, since the probability of a grain-grain collision within this region is about 10^{-3} , the probability of such collisions leading to mantle destruction is $(7 \times 10^6)^{-1} \times 10^{-3} \times 10^{-1} \text{ year}^{-1} \approx 1.4 \times 10^{-11} \text{ year}^{-1}$, or a factor of at least 10^3 smaller than the destruction probability due to the sputtering process. We thus consider it unlikely that direct grain-grain collisions between grains from different clouds are important in the destruction of grain mantles.

Due to the high temperatures behind the shock front, the grain acquires a much larger electric charge than usual, and $Z_{\text{gr}} \gtrsim 30$ for the typical cases considered here. For a preshock magnetic field of 3 microgauss the gyroradius is then $r_g \approx 10^{-4}$ pc and slowly decreases through the cooling region to $\sim 10^{-5}$ pc in the cold, dense region. The gyroradius is therefore small compared with the cooling region, which is 10^{-3} – 10^{-2} pc. A magnetic field of 3 microgauss parallel to the shock front may thus couple the grain effectively to the gas behind the shock front. The grains will be turned around in the gas frame on a timescale $\pi r_g / U \approx 10^2$ years and will undergo many gyrations before they finally come to rest with respect to the gas. This makes possible head-on collisions between grains from one and the same cloud. Furthermore, since the grains now stay with the gas with which they went through the shock front instead of traveling into colder gas, the sputtering rate may increase. However, this may be offset by a smaller grain-to-gas velocity, since the hotter gas has a larger flow velocity.

Finally, we discuss the cooling lines shown in figure 8. The most important molecular hydrogen line for a wide range in shock velocities is the $6.9\text{-}\mu$ ($J = 7 \rightarrow 5$) line of ortho- H_2 . The next strongest line is the $9.7\text{-}\mu$ ($J = 5 \rightarrow 3$) line and then the $8.0\text{-}\mu$ ($J = 6 \rightarrow 4$) line of para- H_2 . Unfortunately, the atmospheric transmission is essentially zero at 6.9μ and only 30–40 percent at 9.7μ (FRAO). It thus seems that the $8.0\text{-}\mu$ line of para- H_2 , which has a transmission of 85–95 percent, is still the best suited for observation as found by FRAO. However, the intensity of the $8.0\text{-}\mu$ line is somewhat reduced from their estimate, since most of the energy appears in the unobservable ortho-lines at 6.9 and 9.7μ . Furthermore, thermal dissociation of H_2 prohibits any increase in the line strength by going to somewhat higher shock speeds. Only if the H_2 abundance in a cloud is $\text{H}_2/\text{H} \gtrsim 0.1$ does it seem that rotational lines of interstellar molecular hydrogen can be observed from the ground.

We see from figure 8 that the oxygen $63\text{-}\mu$ line is the most important atomic line, except at very high shock speeds, $\gtrsim 18 \text{ km s}^{-1}$, where the $6300\text{-}\text{\AA}$ line becomes very strong. The Fe^+ ($26\text{-}\mu$) and Si^+ ($35\text{-}\mu$) lines are somewhat stronger than the C^+ ($156\text{-}\mu$) line, contrary to what was found by FRAO. We attribute this to our slightly different cooling rates (§ V).

It was suggested by FRAO that molecules could rapidly build up in the shock wave until they became important cooling agents, thus prohibiting further formation from taking place. However, we have seen that the abundances of the molecules OH and H_2O are kept low due to rapid destruction mechanisms and never become important cooling agents, accounting for at most a few percent of the total cooling rate. We have found that molecules like CO and CN may build up continuously through the shock front, since they are destroyed mainly by photodissociation on a timescale greater than or equal to the cooling time. On the other hand, vibrational transition probabilities are small and contributions from this process are not expected to be significant. Only if very large multiquantum rotational transitions were to occur in these molecules could they influence the shock structure as we have studied it here.

This research was accomplished while the author held a National Research Council Postdoctoral Resident Research Associateship at the Goddard Institute for Space Studies, New York. The work is based on a thesis submitted in partial fulfillment of

the requirements for a Ph.D. at the University of California, Berkeley, and I wish to thank my adviser, Dr. George B. Field, for suggesting the problem and for his guidance and encouragement. I also wish to acknowledge the helpful discussions with John Hutchins, William Le Jeune Brown, Dr. M. J. Welch, Dr. M. W. Werner, and Dr. W. D. Gwinn. Finally, I wish to thank Paul Woodward for his assistance in running the computer program.

APPENDIX

Figure 9 shows a particle m incident at an angle I upon a surface composed of particles M separated by a distance c . The hard-sphere collision radii are r_m and r_M , respectively. We see that ejection may only occur for angles $\gamma_l < \gamma < \gamma_m$, where $\sin \gamma_l = 2(r_M + r_m)/c$, $\cos \gamma_m = 2r_M/c$. For a given ejection angle γ , there is a minimum angle of incidence I_{\min} for sputtering to occur. If $\alpha \equiv \pi/2 - \gamma$ and $r \equiv r_m + r_M$, one may easily show (Henschke 1957, eq. [4.3]) that

$$c \sin I_{\min} - r \sin (I_{\min} + \alpha) = r. \quad (\text{A1})$$

Equation (A1) may be solved explicitly to give

$$t_g I_{\min} = \frac{\sin \alpha (1 - r/c \cos \alpha) + (1 - 2r/c \cos \alpha)^{1/2}}{c/r - 2 \cos \alpha + r/c \sin^2 \alpha}. \quad (\text{A2})$$

The smallest value of I_{\min} is clearly obtained for $\gamma = \gamma_m$. Denoting this value of I_{\min} for I_0 , we have

$$t_g I_0 = \frac{\cos \gamma_m (1 - r/c \sin \gamma_m) - (1 - 2r/c \sin \gamma_m)^{1/2}}{c/r - 2 \sin \gamma_m + r/c \cos^2 \gamma_m}. \quad (\text{A3})$$

We also see that the maximum value of I is given by $I = I_m = \gamma_m$. Let $I_1 \equiv I_{\min}(\gamma_l) = \gamma_l$ and let the angles of ejection for a given angle of incidence be $\gamma_l \leq \gamma \leq \gamma_m$. We see

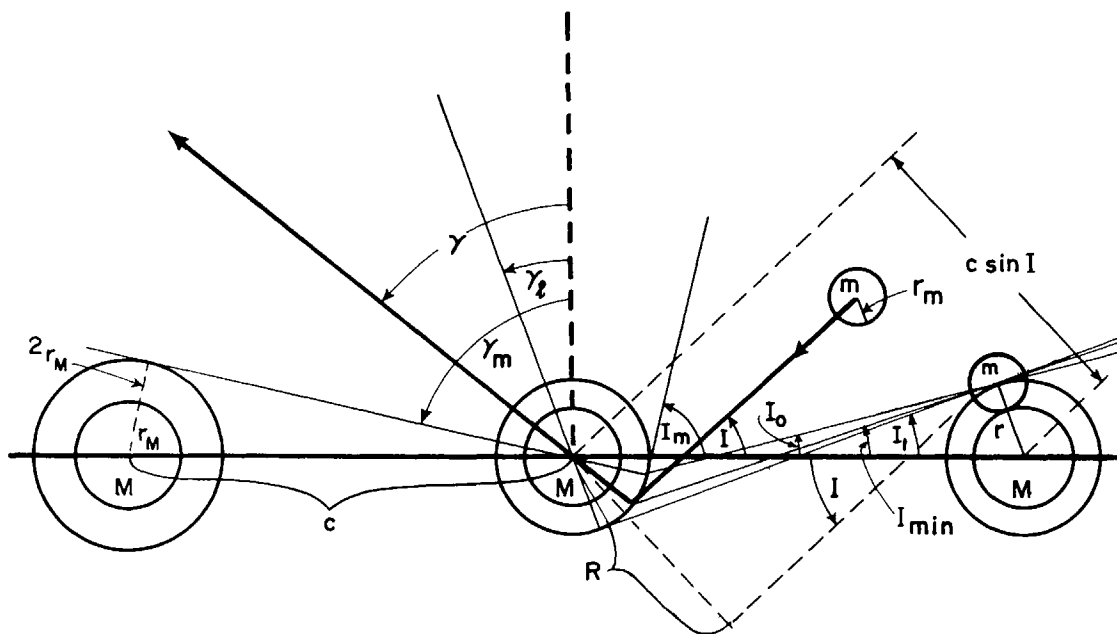


FIG. 9.—Geometry for oblique incidence sputtering

from figure 9 that if $I_0 \leq I \leq I_1$, γ_i is given by equation (A1) in the form

$$c \sin I - r \sin [I + (\pi/2) - \gamma_i] = r, \quad (\text{A4})$$

which may be solved explicitly to give

$$t_g \gamma_i = \frac{-r^2 \sin I \cos I \pm r(c \sin I - r)[1 - (c/r \sin I - 1)^2]^{1/2}}{r^2 \sin^2 I - (c \sin I - r)^2}. \quad (\text{A5})$$

Here we need to use the sign that gives the largest value of γ_i . The second solution for γ_i corresponds to extending the line of incidence to its second intersection with the circle of radius r . If $I_1 \leq I \leq I_m$ we see from figure 9 that $\gamma_i = I$.

The probability of M being sputtered must be proportional to the ratio of the flux of particles m giving ejection angles $\gamma_i \leq \gamma \leq \gamma_m$ to the total flux falling on the sphere with radius r . Since the former is

$$\propto 2r^2 \int_{\gamma_i}^{\gamma_m} \sin \gamma \sin (\gamma - I) d\gamma$$

and the latter is $\propto \pi r^2$, we have for the ratio

$$\begin{aligned} p_0 &= \frac{2}{\pi} \int_{\gamma_i}^{\gamma_m} \sin \gamma \sin (\gamma - I) d\gamma \\ &= \frac{1}{\pi} \cos I (\gamma_m - \gamma_i - \sin \gamma_m \cos \gamma_m + \sin \gamma_i \cos \gamma_i) \\ &\quad - \frac{1}{\pi} \sin I (\sin^2 \gamma_m - \sin^2 \gamma_i). \end{aligned} \quad (\text{A6})$$

The probability p_0 must be modified to take account of the flux that does not hit any surface particle at all. From figure 9 we see that the probability of hitting the target particles is $p = \pi r^2 / \pi R^2 = (r/R)^2$, where $R = c \sin I - r$, provided $R > r$, i.e., $I \geq I_1$. If $I \leq I_1$, the surface particles are shadowed by each other, so that this probability is unity. Thus, the geometric factor in the yield function is

$$P_g(I) = p_0(I)p(I), \quad (\text{A7})$$

where

$$\begin{aligned} p(I) &= (c/r \sin I - 1)^{-2} \quad \text{if} \quad I \geq I_1; \\ &= 1 \quad \text{otherwise.} \end{aligned} \quad (\text{A8})$$

REFERENCES

- Aannestad, P. A. 1973, *Ap. J. Suppl.*, **25**, 205 (Paper I).
 Bahcall, J. N., and Wolf, R. A. 1968, *Ap. J.*, **152**, 701.
 Baines, M. J., Williams, I. P., and Asebiomo, A. S. 1965, *M.N.R.A.S.*, **130**, 63.
 Barlow, M. J. 1971, *Nature Phys. Sci.*, **232**, 152.
 Benedict, W. S., Claassen, H. H., and Shaw, J. H. 1952, *J. Res. N.B.S.*, **49**, 91.
 Broida, H. P., and Carrington, T. 1963, *J. Chem. Phys.*, **38**, 163.
 Callear, A. B., and Lambert, J. D. 1969, *Comprehensive Chemical Kinetics*, ed. C. H. Bamford and C. F. H. Tipper (New York: Elsevier Publishing Co.), p. 233.
 Carroll, T. O., and Salpeter, E. E. 1966, *Ap. J.*, **143**, 609.
 Dean, A. M., and Kistiakowski, G. B. 1971, *J. Chem. Phys.*, **54**, 1718.
 Dieke, G. H., and Crosswhite, H. M. 1962, *J. Quant. Spectrosc. and Rad. Transf.*, **2**, 97.

- Dieter, N. H., and Goss, W. M. 1966, *Rev. Mod. Phys.*, **38**, 256.
 Field, G. B., Aannestad, P. A., and Solomon, P. M. 1968, *Nature*, **217**, 435.
 Field, G. B., Rather, J. D. G., Aannestad, P. A., and Orszag, S. A. 1968, *Ap. J.*, **151**, 953.
 Field, G. B., Sommerville, W. B., and Dressler, K. 1966, *Ann. Rev. Astr. and Ap.*, **4**, 207.
 Foner, S. N. 1966, *Adv. Atomic and Molecular Phys.*, **2**, 385.
 Frisch, P. 1972, *Ap. J.*, **173**, 301.
 Gardiner, W. C., Jr., and Kistiakowski, G. B. 1961, *J. Chem. Phys.*, **35**, 1765.
 Gentieu, E. P., and Mentall, J. E. 1970, *Science*, **169**, 681.
 Gidalevich, E. Ya. 1966a, *Soviet Astr.—AJ*, **9**, 716.
 ———. 1966b, *ibid.*, **10**, 437.
 ———. 1966c, *Astrofizika*, **2**, 155.
 ———. 1967, *Soviet Astr.—AJ*, **10**, 817.
 Goss, W. M. 1967, *Ap. J. Suppl.*, **15**, 131.
 Goss, W. M., and Field, G. B. 1968, *Ap. J.*, **151**, 177.
 Habing, H. J. 1968, *B.A.N.*, **19**, 421.
 Habing, H. J., and Goldsmith, D. W. 1971, *Ap. J.*, **166**, 525.
Handbook of Chemistry and Physics. 1964–65 (45th ed.; Cleveland: Chemical Rubber Co.), p. F94.
 Henschke, E. B. 1957, *Phys. Rev.*, **106**, 737.
 Herzfeld, K. F., and Litovitz, T. A. 1959, *Absorption and Dispersion of Ultrasonic Waves* (New York: Academic Press).
 Hollenbach, D. J., Werner, M. W., and Salpeter, E. E. 1971, *Ap. J.*, **163**, 165.
 Howard, W. E., Wentzel, D. G., and McGee, R. X. 1963, *Ap. J.*, **138**, 988.
 Hurle, I. R. 1967, *Rept. Progr. Phys.*, **30**, 1, 149.
 Johnston, H. S. 1966, *Gas Phase Reaction Rate Theory* (New York: Ronald Press), p. 207.
 Julienne, P. S., Krauss, M., and Donn, B. 1971, *Ap. J.*, **170**, 65.
 Kahn, F. 1955, *Gas Dynamics of Cosmic Clouds*, ed. H. C. van de Hulst and J. M. Burgess (Amsterdam: North-Holland Publishing Co.), chap. 12.
 Klemperer, W. 1971, *Highlights of Astronomy*, Vol. **2**, ed. C. de Jager (Dordrecht, Holland: D. Reidel Publishing Co.), p. 421.
 Kolos, W., and Roothaan, C. C. J. 1960, *Rev. Mod. Phys.*, **32**, 219.
 Kurylo, M. J., Hollinden, G. A., and Timmons, R. B. 1970, *J. Chem. Phys.*, **52**, 1773.
 Kurylo, M. J., and Timmons, R. B. 1969, *J. Chem. Phys.*, **50**, 5076.
 Magee, E. M. 1963, *J. Chem. Phys.*, **39**, 855.
 Marr, G. V. 1967, *Photoionization Processes in Gases* (New York: Academic Press), p. 187.
 Mathews, W. G. 1969, *Ap. J.*, **157**, 583.
 Mayer, S. W., Schieler, L., and Johnston, H. S. 1967, *Proc. Symp. (Internat.) Combustion*, **11**, 837.
 Molchanov, V. A., and Telkovskii, V. G. 1961, *Soviet Phys. Doklady*, **6**, 137.
 Münch, G. 1964, *Ap. J.*, **140**, 107.
 Nash, L. K. 1962, *Elements of Chemical Thermodynamics* (Reading, Mass: Addison-Wesley Publishing Co.), p. 112.
 Nishimura, S. 1968, *Ann. Tokyo Astr. Obs.*, **11**, 33.
 Oort, J. H., and van de Hulst, H. C. 1946, *B.A.N.*, **10**, 187.
 Penston, M. V. 1970, *Ap. J.*, **162**, 771.
 Penzias, A. A., Jefferts, K. B., and Wilson, R. W. 1971, *Ap. J.*, **165**, 229.
 Potter, A. E., and Del Duca, B. 1964, *Icarus*, **3**, 103.
 Rapp, D., and Kassal, T. 1969, *Chem. Rev.*, **69**, 61.
 Schofield, K. 1967, *Planet. and Space Sci.*, **15**, 643.
 Seaton, M. J. 1955, *Ann. d'ap.*, **18**, 188.
 Solomon, P. M., and Werner, M. W. 1971, *Ap. J.*, **164**, 41.
 Spitzer, L., Jr. 1962, *Physics of Fully Ionized Gases* (New York: Interscience Publishers).
 ———. 1968, *Diffuse Matter in Space* (New York: Interscience Publishers).
 Stecher, T. P., and Williams, D. A. 1966, *Ap. J.*, **146**, 88.
 Steinfeld, J. I., and Klemperer, W. 1965, *J. Chem. Phys.*, **42**, 3475.
 Stief, L. J., Donn, B., Glicker, S., Gentieu, E. P., and Mentall, J. E. 1972, *Ap. J.*, **171**, 21.
 Stone, M. E. 1970a, *Ap. J.*, **159**, 277.
 ———. 1970b, *ibid.*, **159**, 293.
 Sun, H., and Weissler, G. L. 1955, *J. Chem. Phys.*, **23**, 1160.
 Takayanagi, K., and Nishimura, S. 1960, *Pub. Astr. Soc. Japan*, **12**, 77.
 Tang, K. T. 1969, *Phys. Rev.*, **187**, 122.
 Wainfan, N., Walker, W. C., and Weissler, G. L. 1955, *Phys. Rev.*, **99**, 542.
 Watanabe, K. 1954, *J. Chem. Phys.*, **22**, 1564.
 ———. 1958, *Adv. Geophys.*, **5**, 198.
 Weaver, H., Williams, D. R. W., Dieter, N. H., and Lum, W. T. 1965, *Nature*, **208**, 29.
 Wehner, G. K. 1959, *J. Appl. Phys.*, **30**, 1762.
 Werner, M. W. 1970, *Ap. Letters*, **6**, 81.

- Whitney, C. A., and Skalafuris, A. J. 1963, *Ap. J.*, **138**, 200.
Wickramasinghe, N. C. 1965, *M.N.R.A.S.*, **131**, 177.
Wiese, W. L., Smith, M. W., and Glennon, B. M. 1966, *Atomic Transition Probabilities*, Vol. **1** (NSRDS-NBS4).
Wilkinson, P. G., and Johnston, H. L. 1950, *J. Chem. Phys.*, **18**, 190.
Williams, D. A. 1970, *Observatory*, **90**, 202.
Wofsy, S., Reid, R. H. G., and Dalgarno, A. 1971, *Ap. J.*, **168**, 161.
Zimmermann, H. 1970, *Astr. Nach.*, **292**, 17.